frontiers | Frontiers in Chemical Engineering

TYPE Original Research
PUBLISHED 25 April 2023
DOI 10.3389/fceng.2023.1145049

OPEN ACCESS

EDITED BY
Hongwei Shi,
Shenyang University of Technology, China

REVIEWED BY
Apurba Sinhamahapatra,
Central Institute of Mining and Fuel Research, India
Sébastien Touzain,
Université de la Rochelle, France

*CORRESPONDENCE
João Tedim,
joao.tedim@ua.pt

RECEIVED 15 January 2023
ACCEPTED 11 April 2023
PUBLISHED 25 April 2023

CITATION
Sushkova A, Montes R, Paulino T, Sousa I, Neves C, Ferreira MGS and Tedim J (2023), A novel smart coating with hexacyanoferrate intercalated layered double hydroxides nanoadditive for early detection of carbon steel corrosion. *Front. Chem. Eng.* 5:1145049. doi: 10.3389/fceng.2023.1145049

A novel smart coating with hexacyanoferrate intercalated layered double hydroxides nanoadditive for early detection of carbon steel corrosion

Alesia Sushkova, Rodrigo Montes, Tiago Paulino, Isabel Sousa, Cristina Neves, Mário G. S. Ferreira and João Tedim*

Department of Materials and Ceramic Engineering, CICECO—Aveiro Institute of Materials, University of Aveiro, Aveiro, Portugal

The detection of corrosion at early stages could increase the service life of metal-based infrastructures in a cost-effective manner. Despite the recent progress in "smart" self-reporting corrosion sensing coatings, the development of environmentally friendly systems appropriate for steel substrate used in offshore applications remains a relevant challenge. In this study, a novel smart corrosion sensing coating, based on hexacyanoferrate intercalated Mg-Al LDH nanoadditive, was developed, aiming at the detection of early-stage corrosion of carbon steel. The detection mechanism is based on the ability of hexacyanoferrate ions to react with iron cations generated during the corrosion process, giving rise to a colorimetric signal, while LDH carriers provide a controlled release of active ions under corrosion conditions. The sensing nanoadditive was embedded into a commercial pigment-free water-based acrylic polyurethane coating. The nanomaterial was characterized structurally (XRD) and morphologically (STEM). The compatibility of the additive with the polymer formulation and its influence on the resulting coating performance was investigated in terms of rheological behavior, structure (FTIR), morphology (SEM/EDS), thermal (TGA, DSC) and mechanical (adhesion, hardness) properties. The corrosion protection ability of the coating was evaluated via EIS, while the sensing functionality was analyzed by visual analysis of the surface. The developed coating successfully detects early-stage corrosion of steel substrate at a lab scale, in conditions relevant to the use of metallic structures in offshore applications, demonstrating a correlation between the level of material degradation and the spectroscopic signal associated with the presence of the LDH functional nanoadditive. Furthermore, the observed decrease in coating barrier properties, caused by the presence of LDH, was overcome by the subsequent development of a multilayer coating system. Two different topcoats (epoxy- and polyurethane-based) were surveyed for this purpose, showing an improvement in the coating barrier properties without influencing the corrosion detection functionality of the sensing layer. The results were successfully validated by standard salt spray tests. The multilayer approach opens up the possibility to model coatings with different characteristics for various operating conditions.

KEYWORDS

corrosion, coating, nanoadditive, detection, layered double hydroxides (LDH), hexacyanoferrate, composite

1 Introduction

Metal corrosion is a global problem, which causes high economic losses in all industries. Annual direct corrosion costs were estimated at about 2.5 trillion USD, corresponding to over 3.4% of the world's gross domestic product (Koch et al., 2016), and continue to grow every year. Furthermore, corrosion poses high indirect risks and costs, such as production delays, health, and environmental hazard effects. Metal corrosion leads to the loss of functionality and durability of metal structures and has a high damage potential, leading to industrial disasters (Niazi et al., 2021) and environmental pollution issues (Ikechukwu and Pauline, 2015). As a result, the development of effective corrosion control methods has been actively investigated over the past decades (Twite and Bierwagen, 1998; Melchers, 2006; Montemor, 2014; Umoren and Solomon, 2019; Zhang et al., 2022; Chen et al., 2023). Moreover, the problem of corrosion is specifically acute in offshore applications, where metal structures are constantly exposed to harsh environments, namely, seawater and UV radiation (Melchers, 2006; Kirchgeorg et al., 2018; Olajire, 2018; Eom et al., 2020).

The application of protective coatings is the most used approach for corrosion prevention. Convenient coatings render a physical barrier effect, capable of avert contact between an environment and the metal structure. However, during service life, the coating itself is subject to degradation, due to single and/or combined factors, including exposure to aggressive environments, mechanical damages, and temperature gradients, among others. The degradation leads to the appearance of defects through the coating, allowing penetration of aggressive ions, water molecules, and oxygen, which, when reaching the metal surface, cause the initiation of corrosion processes. In this context, the development of smart coatings capable of providing corrosion responsive functionalities has been under consideration by several research groups (Montemor, 2014; Ulaeto et al., 2017; Lv et al., 2021b; Habib et al., 2021; Chen et al., 2023). One of the research branches in this direction is the development of coatings capable to detect/signal corrosion at an early stage, when metal degradation is still small and invisible to the naked eye (Ma et al., 2021). The ability of early detection of corrosion can be, both alone or when combined with other structural health monitoring techniques, a cost-effective strategy to reduce maintenance costs and risks associated with catastrophic failure of structures, contributing for the overall extension of the service life of metallic structures.

Steel is one of the most frequently used metals in many industries, due to its high strength, and durability (Melchers, 2006; Farjana et al., 2021). Steel is capable to withstand high temperatures and severe stress, herewith it is relatively cheap. However, corrosion leads to a deterioration of steel mechanical properties and consequential premature aging of steel-based infrastructures. Detection of steel corrosion at an early stage allows the application of maintenance measures in a timely manner, preventing irreparable material destruction and construction failure. Recently, developed corrosion-responsive protective coatings enabled corrosion spotting, while the degradation is still invisible to the naked eye (Ma et al., 2021). In contrast to the other proposed methods for the detection of corrosion initiation, such as ultrasonic inspection (Hogg et al., 2019), radiography and gammatography (Priyada et al., 2011), employment of electrochemical (Xia et al., 2022) and magnetic sensors (Tsukada et al., 2018), optical fiber (Tan et al., 2021), and thermal imaging (Raverkar et al., 2021), the application of corrosion sensing coatings allows continuous monitoring of surface conditions without any expensive equipment. The detection mechanism is, hence, autonomous and based on the impregnation of active agents, capable of reacting with the species formed during the corrosion process, giving a noticeable self-reporting signal inside the coating matrix.

The corrosion of carbon steel in the presence of chloride-based electrolytes under neutral pH conditions can be described by a set of electrochemical processes that induce local changes at the surface of the material, namely, the oxidation of the metal substrate (Eq. 1) and reduction of oxygen or water (Eqs. 2, 3) (Revie and Uhlig, 2008):

$$Fe \leftrightarrow Fe^{2+} + 2e^{-} \tag{1}$$

$$O_2 + 2H_2O + 4e^{-} \leftrightarrow 4HO^{-} \tag{2}$$

$$2H_2O + 2e^{-} \leftrightarrow H_2 + 2OH^{-} \tag{3}$$

Looking at the type of species formed during corrosion processes, one can focus on the detection of those formed from the anodic or cathodic half-reactions, namely, the metal cations or hydroxides. In fact, pH indicators such as phenolphthalein (Frankel and Zhang, 1999; Maia et al., 2013), coumarin (Wang et al., 2018), fluorescent dyes (Theerasilp and Crespy, 2021), and other pH-sensing compounds have been proposed in the literature for implementation of corrosion detection coatings for different metal alloys. These compounds show the ability to detect early-stage corrosion by reacting with the hydroxides formed in the cathodic half-reaction of the corrosion process, giving a colorimetric signal. Encapsulation of the sensing additives in nano- and microcarriers was applied to increase their compatibility with the coatings and provide a controlled release of the active compounds (Li and Calle, 2007; Maia et al., 2013; Sousa et al., 2020). Despite the success in corrosion detection of pH-sensing coatings under atmospheric and aqueous sodium chloride conditions, their employment in offshore applications could be challenging, due to the alkaline nature of the seawater. The average global ocean surface pH is about 8.1, and in some regions even reaches pH 9.0 (Halevy and Bachan, 2017), which could interfere with the detection mechanism of the coating, giving a false positive signal. Another challenge can arise from the fact that changes in pH may vary remarkably, depending on whether corrosion processes are localized or uniform (Bastos et al., 2010).

An alternative corrosion-sensing mechanism for protective coatings, recently investigated, is based on the reaction of the embedded active compounds with iron cations formed in the anodic half-reaction of the corrosion process. Ferric species indicators Rhodamine B derivatives (Augustyniak et al., 2009), 8-

hydroxyquinoline (Roshan et al., 2018), and phenanthroline (Dhole et al., 2015; Cao et al., 2022) have been proposed as active agents in corrosion-sensing coatings for steel. These compounds showed the ability to detect early-stage corrosion by giving fluorescence or color-change signals. In recent studies, Rhodamine B derivatives were immobilized in silica capsules (Exbrayat et al., 2019), zeolites (Lv, et al., 2021a), and layered double hydroxides (LDH) (Lv, et al., 2021b), and 8-hydroxyquinoline in polyaniline microcapsules (Taheri et al., 2022), demonstrating good corrosion-detection performance. However, these compounds showed high toxicity towards marine organisms (Feldmannová et al., 2006; Yan et al., 2015; Skjolding et al., 2021), which may limit their use in contact with aquatic compartments.

In our recent work (Wilhelm et al., 2020), we proposed a novel active nanoadditive for early detection of steel corrosion–hexacyanoferrate intercalated LDH (Mg-Al/$[Fe(CN)_6]$ LDH). LDH were used as hosting material for hexacyanoferrate (III) ions, able to provide controlled release of the active agent through the ion exchange mechanism under the conditions associated with the onset of corrosion. The released hexacyanoferrate ions can react with iron cations formed during corrosion of steel, providing a strong colorimetric signal–the formation of blue precipitates (Prussian Blue and Turnbull's Blue). The detection ability was confirmed on uncoated carbon steel plates immersed in a chloride-containing solution with the sensing nanoadditive (Wilhelm et al., 2020). Furthermore, the toxicity of the developed nanoadditive was assessed in terms of environmental fate and behavior using the marine microalgae *Tetraselmis chuii* and the crustacean *Artemia salina* (Martins et al., 2022). Mg-Al/$[Fe(CN)_6]$ LDH, as well as free hexacyanoferrate, did not show toxicity for *Artemia salina* up to the highest tested concentration (100 mg/L). A low toxic effect of free hexacyanoferrate ion on *Tetraselmis chuii* was detected, meanwhile, the immobilization of the active anion in the LDH reduced the toxicity by 33%.

Having set that Mg-Al LDH intercalated with hexacyanoferrate ions are able to detect corrosion of carbon steel and exhibit low toxicity for aquatic organisms, the next step is to test these nanoadditives inside protective coatings. In the present work, we report the development of a new corrosion-sensing protective coating based on the proposed environmentally friendly sensing nanoadditive Mg-Al/$[Fe(CN)_6]$ LDH and water-based acrylic polyurethane (so-called sensing layer), and subsequent development of a multilayer coating system with additional topcoat for improving barrier properties of the overall sensing coating system, based on polyurethane and epoxy-based chemistries. To the best of our knowledge, no studies on sensing coatings based on hexacyanoferrate intercalated LDH have been reported in the literature.

2 Materials and methods

2.1 Materials

Potassium hexacyanoferrate (III) (Riedel de Haën), Mg-Al/NO_3 LDH (Mg/Al = 2) (Smallmatek Lda.), sodium chloride (Sigma-Aldrich), iron (II) lactate (Sigma-Aldrich), iron (II) chloride tetrahydrate (Fluka), iron (III) chloride hexahydrate (Sigma-Aldrich), iron (III) nitrate nonahydrate (Sigma-Aldrich), sodium hydroxide (eka), acetone (Riedel de Haën), water-based acrylic polyurethane coating precursor AQ CC 80 (SYNPO, akciová společnost), solvent-based acrylic polyurethane coating precursor LV CC 100 (SYNPO, akciová společnost), coating hardener AQ BU 16 (SYNPO, akciová společnost), coating hardener LV BU 45 N (SYNPO, akciová společnost), solvent-based epoxy varnish 2K 5-0282 (Duquebel), varnish hardener 2K 5-0260 (Duquebel), Pro-Reef meersalz/sea salt (Tropic Marin), and buffer pH 9 solution (Carlo Erba) were used as received.

2.2 Sensing nanoadditive

Mg-Al/$[Fe(CN)_6]$ LDH sensing nanoadditive was synthesized as described in our previous work (Wilhelm et al., 2020). Hexacyanoferrate (III) anions were intercalated in LDH nanocarriers by a one-step ion-exchange process using potassium hexacyanoferrate (III) salt and Mg-Al nitrate intercalated LDH, with Mg:Al ratio equal 2:1, as precursor materials. 7.5 g (dry mass) of Mg-Al/NO_3 LDH in form of water-based slurry was dispersed in 0.1 M aqueous solution of $K_3[Fe(CN)_6]$ (0.25 L) and stirred for 24 h. The resulting suspension was filtered and washed with distilled water.

The details on the development of Mg-Al/$[Fe(CN)_6]$ LDH sensing nanoadditive, its characterization, as well as the characterization of the precursor materials and functionality tests, are presented in our previously published paper (Wilhelm et al., 2020). In the frame of this work, the morphology of the developed nanoadditive and precursor Mg-Al/NO_3 LDH has been explored in more detail via Scanning Transmission Electron Microscope (STEM) Hitachi HD-2700, using secondary electron imaging mode and bright field transmission imaging mode, under the electron beam energy of 200 kV. The structure of the nanoadditive was confirmed by X-Ray diffraction (XRD) of dried LDH powder, using X´Pert PRO^3 (Malvern Panalytical) diffractometer with Cu Kα radiation (λ = 1.5418 Å) and graphite monochromator. The diffractograms were processed using HighScore Plus software.

2.3 Development of the sensing layer

2.3.1 Development of the sensing coating formulation

Commercially available water-based acrylic urethane emulsion AQ CC 80 with 35 wt% solid content, supplied by SYNPO, was used for the preparation of sensing coating formulations. It was chosen due to its environmental friendliness–crucially lower and less toxic emissions of volatile organic compounds than in solvent-based formulations (the content of organic solvents in the mixed coating is less than 150 g/L) and good performance of the resulting coating (adhesion to the carbon steel substrate, barrier properties, and transparency).

Mg-Al/$[Fe(CN)_6]$ LDH sensing nanoadditive was added to the AQ CC 80 emulsion in form of a water-based slurry (w_{solid} = 21.6 wt%) in mass concentrations of 10, 5, and 0 (reference sample) wt%. The ratio of the additive in the formulation was calculated

considering the mass of dry particles to the mass of solids content in the formulation. To estimate the influence of the intercalation of the active ions inside the LDH on the resulting coating performance, hexacyanoferrate in the form of potassium salt was dispersed in the AQ CC 80 emulsion in a concentration corresponding to the loading content of $[Fe(CN)_6]^{3-}$ in the formulation with 5 wt% of Mg-Al/$[Fe(CN)_6]$ LDH additive, which corresponds to ca. 1.3 wt% of $K_3[Fe(CN)_6]$ nanoadditive. The formulations were investigated considering different parameters to obtain a well-dispersed, stable emulsion. The dispersion of the particles in the main component of the polymeric coating formulation was achieved by stirring with a magnet at 300 rpm for half an hour followed by ultrasound treatment (ultrasound water bath) for around 1 h at 50 Hz.

2.3.2 Testing of the compatibility of the nanoadditive with the coating formulation

The possibility of the sensing nanoadditive to detect iron cations inside the coating formulation was tested on the prepared liquid formulations by the addition of Fe^{2+} salt cations in form of iron (II) lactate and subsequent visual inspection.

The influence of the nanoadditive on the coating performance was analyzed in terms of viscosity and viscoelastic behavior. The rheological study was performed on a Kinexus lab + rotational rheometer (Malvern), using a 4° cone geometry with a diameter of 40 mm and a gap of 150 μm (CP4/40 SR2216 SS). The viscosity of formulations was analyzed in rotational mode using a shear rate sweep between 1 and 1,000.0 s^{-1}, measuring 10 points per decade. The yield stress was analyzed in a shear stress ramp from 0.1 to 100 Pa, measuring 10 points per decade as well. The viscoelastic properties of the formulations were studied using a constant shear strain of 2% at a frequency sweep from 1 to 10 Hz. The shear strain corresponding to the linear viscoelastic region was determined after performing an amplitude sweep with shear stress from 0.1 to 10 Pa, frequency—1 Hz, measuring 10 points per decade. All the analyses were performed at the constant temperature of 25°C.

2.3.3 Pre-treatment of steel substrate

Standard test carbon steel plates commercially available as Q-LAB Q-panel (type S - 46) with a thickness of 0.81 mm were used as the substrate for coatings application. The chemical composition is Mn ≤ 0.60 wt%, C ≤ 0.15 wt%, S ≤ 0.035 wt%, p ≤ 0.030 wt%, and Fe (balance). The surface of each plate has been treated before coating application to provide uniformity. Polishing of the samples was performed using Buehler Cabinet sandpapers starting from P 320, gradually increasing, and finishing with P 1000, to reach a straight, homogeneous, flat, and leveled surface. Afterwards, the plates were washed with acetone and dried with compressed air.

2.3.4 Coating preparation

The formulations prepared in Section 2.3.1 were mixed with the hardener (AQ BU 16, SYNPO), with a formulation/hardener mass ratio of 5:2, as described in the product technical. AQ BU 16 was smoothly added to the solution with gentle stirring with a spatula, followed by magnetic stirring at 200 rpm during 5 min to achieve homogeneous mixing. The coatings were applied on a pre-treated carbon steel substrate (Section 2.3.3) using a gap film applicator with a 200 μm gap. The resulting wet films were left to dry in the air at room temperature (20°C ± 2°C) for approximately 2 h and then cured in an oven at 80°C for 1 h.

2.3.5 Investigation of the corrosion detection functionality and corrosion protection performance of the sensing layer

First, the sensing functionality of the prepared coatings was evaluated by an immersion test of the coated substrates in 0.05 M NaCl solution, followed by visual monitoring of the corrosion processes. Then, the corrosion detection functionality and coating protective performance of the selected systems were tested at a lab scale by immersion of the coated steel plates in 0.6 M NaCl solution (condition equivalent to the average salinity of seawater). A coating with 5 wt% sensing nanoadditive was compared with the reference sample (without the nanoadditive) and with a coating with hexacyanoferrate in the form of potassium salt. Electrochemical impedance spectroscopy (EIS) was used to monitor the evolution of the corrosion process in the absence and presence of the sensing nanoadditive using a Gamry potentiostat/galvanostat/zero resistance ammeter Interface 1000 at open circuit potential with an applied sinusoidal perturbation of 10 mV, in the frequency range from 10^5 to 10^{-2} Hz, measuring 7 points per decade over a surface area of 3.46 cm^2. A cell composed of a saturated calomel reference electrode, a platinum foil as a counter electrode, and the coated steel substrate, with or without Mg-Al/$[Fe(CN)_6]$ LDH sensing nanoadditive, as the working electrode. The corrosion detection functionality of the coating was monitored in between EIS measurements by visual analysis of the surface using a stereo microscope Nikon SMZ18. All the immersion tests were performed at room temperature (20°C ± 2°C). To ensure reproducibility of the results at least 3 samples of each system were investigated. The dry thickness of the coatings was evaluated using an Elcometer 456 coating thickness gauge, measuring at least 10 points for each plate (in various parts of the surface).

2.3.6 Investigation of the structure and morphology of the sensing layer

The morphology of the cured coatings was analyzed using a stereo microscope Nikon SMZ18 with magnification up to ×13.5 and a scanning electron microscope (SEM) Hitachi SU-70, operated at 15.0 kV. Elemental mapping of the surface and cross-section of the coatings was performed via energy dispersive spectroscopy (EDS) on the SEM.

The structure of coatings was analyzed via Attenuated Total Reflectance Fourier Transform Infrared (ATR-FTIR) spectrometry using a Bruker Optics tensor 27 Fourier Transform-IR spectrometer, equipped with a Golden Gate ATR accessory plate. For this purpose, coatings were prepared as separate films by applying coating formulations on Teflon substrates, using the same protocol as described at Section 2.3.4, followed by peeling off the cured films. The spectra were collected at ambient conditions of pressure and temperature in a wavenumber range from 4,000 to 500 cm^{-1} with a resolution of 2 cm^{-1}.

2.3.7 Investigation of the thermal properties of the sensing layer

Thermal stability of the sensing layer and the reference coating was studied by thermogravimetric analysis (TGA) in N_2 atmosphere

by heating from room temperature to 500°C, with heating rate 10°C/min, using Simultaneous Thermogravimetric Analyzers NEXTA STA 300 (Hitachi). The sampling mass was about 8.5–9.5 mg. The analysis was performed on the coatings prepared as separated films, as described in Section 2.3.7. The glass transition temperature (T_g) of the coatings was investigated using differential scanning calorimetry (DSC) on Power Compensation Dynamic Scanning Calorimeter Perkin Elmer Diamond according to International Standard ISO 11357-2: "Plastics—Differential scanning calorimetry (DSC) — Part 2: Determination of glass transition temperature and step heigh" (ISO, 2020). The analysis was performed in Al crucibles, measuring specific heat (C_p) via heat-cool method in the temperature range from −20°C to 95°C with heating/cooling rate 20°C/min. Second heating run data was used for the investigation of T_g.

2.3.8 Investigation of the influence of the sensing additive on mechanical properties of the coating

Adhesion of the sensing layer to the steel substrate was tested according to ASTM D3359 "Standard test methods for rating adhesion by tape test" (ASTM, 2022), using the TQC Cross Cut Adhesion Test KIT CC1000. Two series of parallel cuts cross angled to each other were made to obtain a pattern of 25 similar squares. The ruled area was evaluated by using the standard table chart (ASTM, 2022) after a short treatment with a stiff brush and adhesive tape.

The hardness of the sensing layer was evaluated using a Micro Vickers Hardness Tester Shimadzu Type M. A regular four-sided diamond pyramid with a 136° angle between opposite faces was pressed into the test material for 15 s under a range of loads (25, 50, and 100 g). At least five indentations were performed at each load. The resulting indentations were analyzed and measured using a calibrated stereo microscope Nikon SMZ18 with magnification up to ×13.5.

2.4 Development of the multilayer coatings

2.4.1 Preparation of the multilayer coating systems

To enhance the barrier effect rendered by the organic coating, a multilayer coating system was developed, with the sensing layer (acrylic polyurethane AQ CC 80 coating with Mg-Al/$[Fe(CN)_6]$ LDH nanoadditive) applied directly onto the metal substrate, followed by the application of an additional protective topcoat without any additives. Several commercial coatings were studied as possible topcoats, among which two were ultimately selected: a solvent-based transparent epoxy varnish (2K 5-0282 from Duquebel) and a solvent-based transparent polyurethane topcoat (LV CC 100 from SYNPO).

To prepare samples for standardized salt spray testing—a standard corrosion test method, used to check corrosion resistance of coated samples, a bar coater suitable for larger coating areas with respect to the lab-scale samples reported in Section 2.3.4 had to be used to cover the entire surface of a 10 cm × 14 cm steel plate. The maximum wet thickness that could be used with the available bar coaters in our lab for this specimen size was 50 µm. Thus, to compensate for the signal loss due to thinning of the sensing layer with respect to the lab studies, where a small coater with a 200 µm gap was used, the LDH concentration in the sensing layer was increased up to 10 wt%. Therefore, for the preparation of a multilayer system, first, the sensing layer was applied with a wet thickness of 50 µm and cured as described in Section 2.3.4, then the epoxy or polyurethane coating was applied on top of it with the same wet thickness and cured according to the manufacturer's instructions (Supplementary Table S1). A coating hardener LV BU 45 N (SYNPO, akciová společnost) was used for curing the polyurethane topcoat, and a varnish hardener 2K 5-0260 (Duquebel) was used for the epoxy topcoat. The steel substrate was prepared by the same procedure as described in Section 2.3.3.

2.4.2 Investigation of the corrosion-protective performance and the sensing functionality of the multilayer coating systems

The corrosion protective performance and the sensing functionality of the multilayer protective coating systems were evaluated at a lab scale by electrochemical and visual monitoring of the corrosion process of the coated steel plates immersed in 0.6 M NaCl solution at room temperature (20°C ± 2°C), using the same methodology as described above in Section 2.3.5. The dry thickness of the coating systems was measured by the coating thickness gauge using the same procedure as described in Section 2.3.5.

2.4.3 Characterization of the multilayer coating systems

Microstructure and morphology of the multilayer coating systems were investigated by the stereo microscope Nikon SMZ18 and SEM SU-70 (Hitachi) operated at 15.0 kV. Elemental mapping was performed via EDS.

The adhesion of the multilayer coating systems to the steel substrate was tested using a TQC Cross Cut Adhesion Test KIT CC1000 according to ASTM D3359 (ASTM, 2022) as described in Section 2.3.8.

2.5 Validation of the corrosion sensing functionality

The results on corrosion-protective performance and the sensing functionality of the multilayer systems were validated by salt spray test—a standardized accelerated corrosion test for validation of the corrosion protection performance of a protective coating by simulation of a corrosive saline environment in a laboratory. The test was performed according to the International Standard ISO 9227: "Corrosion tests in artificial atmospheres–salt spray tests" (ISO and CEN, 2022), accompanied by a visual assessment of the coating surfaces. The test was performed in a salt spray chamber using the operating conditions specified for neutral salt spray: the temperature was held at 35°C ± 2°C, the concentration of NaCl was 50 ± 5 g/L.

3 Results

3.1 Corrosion-sensing nanoadditive

Hexacyanoferrate intercalated Mg-Al LDH were selected to be used as the functional nanoadditive for the detection of early-

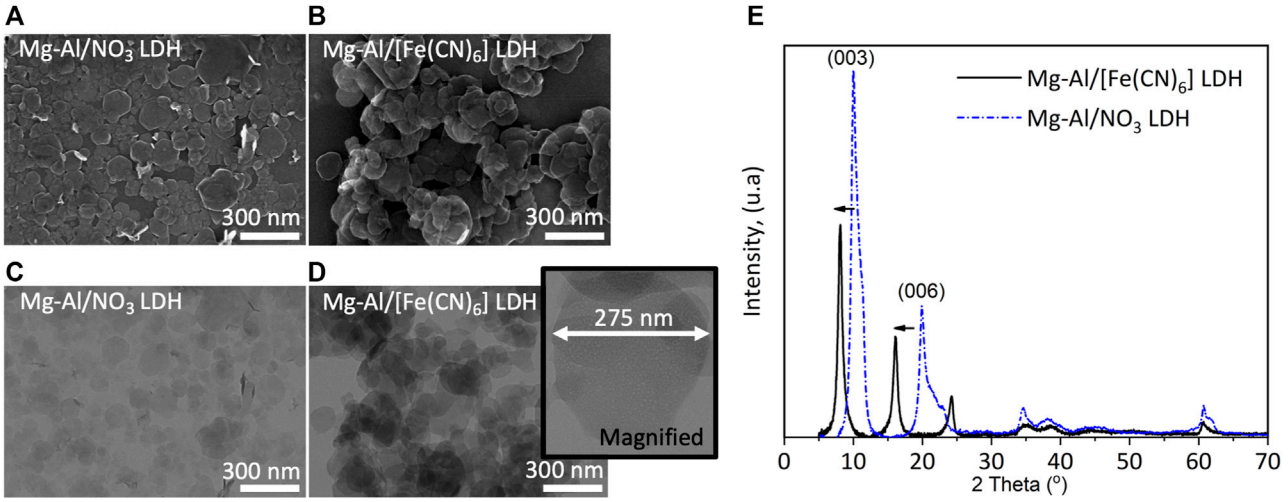

FIGURE 1
Characterization of corrosion-sensing nanoadditive Mg-Al/$[Fe(CN)_6]$ LDH and precursor Mg-Al/NO_3 LDH: STEM via secondary electron imaging mode **(A, B)**, STEM via bright field transmission imaging mode **(C, D)**, and XRD **(E)**.

stage corrosion of steel. The results of the characterization of the synthesized Mg-Al/$[Fe(CN)_6]$ LDH and the precursor Mg-Al/NO_3 LDH and the assessment of the functionality of the sensing nanoadditive are presented in our previously published paper (Wilhelm et al., 2020). In summary, materials were investigated structurally via X-ray diffraction and FTIR, while the morphology of the particles was observed by SEM. The loading content of the hexacyanoferrate ion in the LDH was evaluated via UV-Visible spectroscopy, and confirmed by gravimetric analysis, and was found to be 17.2 wt%. The release of the hexacyanoferrate ions was studied in various aqueous media using UV-Vis spectroscopy (a typical representation of the UV-Visible spectra is shown in Supplementary Figure S1). The LDH showed the ability to respond to the conditions relevant for corrosion (presence of hydroxide ions and chlorides), allowing controlled release of the active anions. The detection functionality of the nanoadditive and its influence on the steel corrosion process was analyzed in a model chloride-containing solution on an uncoated carbon steel substrate using electrochemical characterization and visual assessment. The nanoadditive confirmed its ability to detect corrosion of steel in dilute NaCl solutions.

In the frame of the present work, the morphology of Mg-Al/$[Fe(CN)_6]$ LDH and precursor Mg-Al/NO_3 LDH were further analyzed via STEM (Figures 1A–D). Observation of the particles in secondary electron imaging mode (Figures 1A, B) confirmed a typical platelet shape of the LDH, showing ultrathin two-dimensional layers placed parallel to the TEM grid. The sensing additive demonstrated a relatively large distribution in particle size, from around 50 to almost 300 nm, with a calculated average particle size diameter of 143 ± 4 nm (size distribution histogram calculated from STEM data using ImageJ software is presented in Supplementary Figure S2). Observation of materials in the transmission imaging mode (Figures 1C, D) highlighted the mass density difference between precursor Mg-Al/NO_3 LDH (Figure 1C) and LDH loaded with hexacyanoferrate ions (Figure 1D). Mg-Al/$[Fe(CN)_6]$ LDH appear darker corresponding to the denser material. Observation of the particles at high magnification (×200,000) revealed a porous structure of the surface (magnified region of Figure 1D).

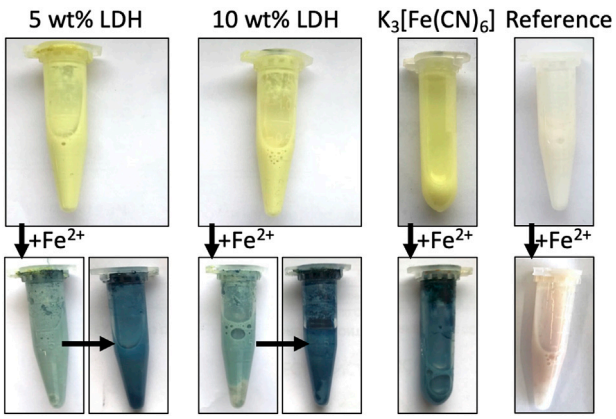

FIGURE 2
Functionality test of the acrylic urethane coating formulation (AQ CC 80) with 5 and 10 wt% of Mg-Al/$[Fe(CN)_6]$ LDH nanoadditive compared to the reference sample and formulation with 1.3 wt% of $K_3[Fe(CN)_6]$ additive.

XRD patterns of the sensing nanoadditive and the precursor LDH are demonstrated in Figure 1E. The observed shift of the peaks corresponding to (003) and (006) reflections towards low angles is associated with the increase of the interlayer distance in the LDH, caused by the replacement of nitrate anions with larger hexacyanoferrate anions. The obtained basal spacings, d_{003}, is 10.9 Å for Mg-Al/$[Fe(CN)_6]$ LDH and 8.8 Å for Mg-Al/NO_3 LDH, which is consistent with the literature data for intercalated

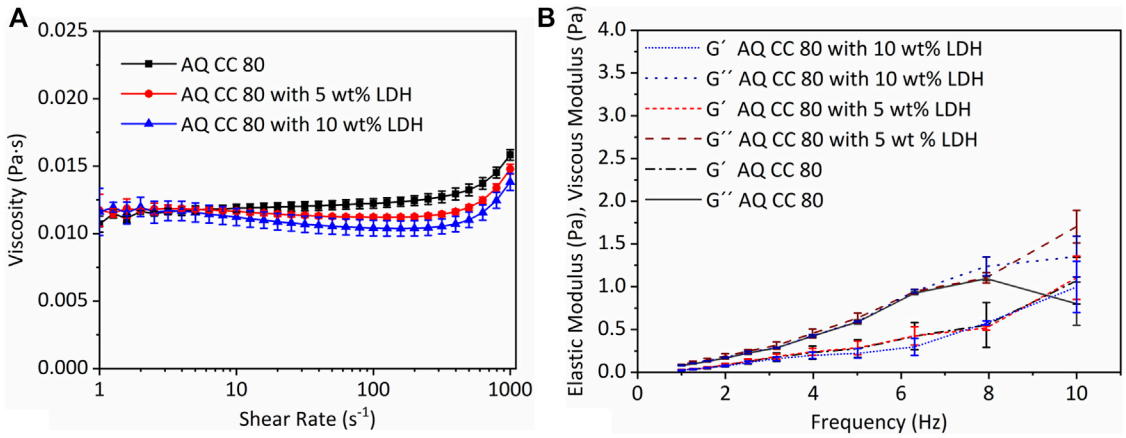

FIGURE 3
Influence of the Mg-Al/$[Fe(CN)_6]$ LDH sensing nanoadditive on rotational **(A)** and oscillatory **(B)** rheological properties of the water-based acrylic urethane coating formulation (AQ CC 80), where G′ is elastic (storage) modulus, G´´ is viscous (loss) modulus.

hexacyanoferrate (Hansen, 1994; Holgado et al., 1996) and nitrate (Cavani et al., 1991) anions, respectively.

3.2 Corrosion-sensing layer

3.2.1 Compatibility of the nanoadditive with the coating formulation

3.2.1.1 Functionality tests

The formulations based on the commercial acrylic urethane emulsion (AQ CC 80) and Mg-Al/$[Fe(CN)_6]$ LDH nanoadditive were prepared and investigated. The compatibility of the sensing nanoadditive with the coating components was examined by means of a functionality test, consisting of the addition of Fe^{2+} cations to the coating formulation with 5 and 10 wt% Mg-Al/$[Fe(CN)_6]$ LDH nanoadditive. For comparison, the same test was performed with the reference formulation (without nanoadditive) and with a formulation with hexacyanoferrate dispersed directly in the emulsion in form of potassium salt in a concentration equal to its content in the solution with 5 wt% LDH nanoadditive (≈1.3 wt% $K_3[Fe(CN)_6]$ additive). Mg-Al/$[Fe(CN)_6]$ LDH were able to detect Fe^{2+} cations by revealing a blue color (Figure 2), while the reference formulation remained white. The appearance of a slight brownish hue observed in the reference sample could be related to the formation of iron hydroxide. After the addition of the iron salt, the color change occurred immediately in all the samples with hexacyanoferrate. However, in the formulations with the hexacyanoferrate ions intercalated in the LDH, the color was initially light blue and intensified after a couple of hours, while in the case of the hexacyanoferrate salt dispersed directly in the solution, the color turned to dark blue immediately after addition of Fe^{2+} cations, and the intensity did not change with time. The blue color in the case of the 10 wt% concentration of the LDH nanoadditive was slightly more intense compared to the 5 wt%.

3.2.1.2 Rheology studies

The rotational rheological properties of the developed formulations were tested in the conditions typically found during coating application, namely, for shear rates between 1 and 1,000 s^{-1} (Figure 3A). The addition of the Mg-Al/$[Fe(CN)_6]$ LDH sensing nanoadditive in the tested concentration (up to 10 wt%) shows no significant effect on the viscosity behavior of the original (reference) formulation. The profiles obtained are very similar with only a slight decrease in viscosity in relation to the reference formulation at the high shear rates, reaching the maximum of 1 mPa s for the formulation with 5 wt% LDH nanoadditive and 2 mPa s for the formulation with 10 wt% LDH nanoadditive at the shear rate 1,000 s^{-1}. This minor difference is most likely associated with the water present in the additive slurry (w_{water} = 78.4 wt%) and does not influence the film application process. Furthermore, it could have a positive effect on decreasing particle aggregation effects (Galvão et al., 2018).

Frequency sweep experiments were performed to determine the response of the formulation for different oscillation timescales (Figure 3B). The viscoelastic profiles confirm the liquid-like behavior of the formulations, as was expected for a waterborne urethane emulsion with 35 wt% solid content (Madbouly et al., 2005). The loss (viscous/liquid-like) modulus G″ dominate the storage (elastic/solid-like) modulus G' up to 9 Hz frequency (Figure 3B) for all the tested formulations, and the phase angle between input stress and the measured strain is out of phase (higher than 45° up to 9 Hz and tends to 90° at rest, 0 Hz) (Supplementary Figure S3). The addition of the LDH slightly increases the gel point of the original coating formulation, up to the point at which the storage modulus becomes higher than the loss modulus and the material loses fluidity. However, the difference lies within the experimental error. The amplitude sweep experiments confirmed that the nanoadditive does not affect the stability of the system (Supplementary Figure S4).

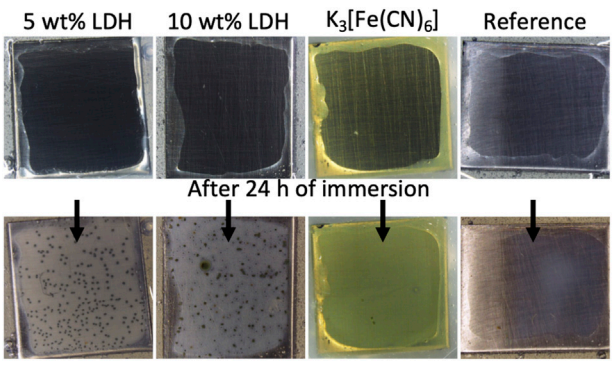

FIGURE 4
Visual analysis of the surface of the coated steel plates before and after immersion in 0.05 M NaCl solution for 24 h.

3.2.2 Coating with the sensing nanoadditive

3.2.2.1 Corrosion sensing and corrosion protection performance of the sensing layer

The acrylic polyurethane coatings formulations (Section 2.3.1) were applied on pre-treated steel plates (Section 2.3.3) and cured as described in Section 2.3.4. The resulting dry thickness of the coatings, measured by the coating thickness gauge, was found to be about 50 ± 5 μm, with a slight decrease of the coating thickness for samples prepared with the LDH compared to the reference coating, which can be associated with the high content of water in the additive slurry. The difference between the wet and dry thickness could be associated with removal of water during the curing process. The coated plates were cut to ~1.5 cm × 1.5 cm and immersed in 0.05 M NaCl solution to accelerate the corrosion process and test their corrosion-sensing ability (Figure 4). The coating with hexacyanoferrate embedded in LDH nanoadditive were compared with the coating prepared by direct dispersion of hexacyanoferrate ion in form of potassium salt into the coating formulation and with the reference coating (without additives). After 24 h of immersion, the acrylic polyurethane AQ CC 80 coating with Mg-Al/$[Fe(CN)_6]$ LDH sensing nanoadditive showed the appearance of a clear colorimetric signal (blue spots), associated with the formation of Prussian/Turnbull's Blue precipitate, while in the reference sample, a corrosion spot barely visible to the naked eye was observed. At the same time, the coating with $K_3[Fe(CN)_6]$ showed a very low signal. Increasing the concentration of the Mg-Al/$[Fe(CN)_6]$ LDH nanoadditive from 5 to 10 wt% did not give a significant visual difference in the signal, thereby the one with the lower percentage was selected for further investigation.

The selected coated steel plates were further studied by EIS to follow the corrosion process and investigate the correlation between the optical signal revealed over time and the level of substrate degradation in the presence and absence of the LDH nanoadditive (Figures 5, 6). The corrosion process was accelerated by immersion of the samples in 0.6 M NaCl solution. The results obtained agree with the preliminary immersion tests described earlier in Figure 4. In the steel plates with the reference coating, corrosion spots invisible to the naked eye (<0.1 mm) were observed via stereo microscope at ×4 after 8 h of immersion (Figure 5B). One corrosion spot became visible to the naked eye after 24 h, and after 1 week at least three corrosion spots were already observed (Figure 5A). For the coating with $K_3[Fe(CN)_6]$ a few greenish/blue spots were observed under a magnifying lens after 24 h of immersion. After 48 h these spots increased in size, becoming visible to the naked eye (Figure 5A). However, several corrosion spots were observed prior to the appearance of the blue colorimetric signal. More detailed photos of the surface of the coating are provided in the Supplementary Material (Supplementary Figure S5). From the tested steel plates coated with the sensing layer (with 5 wt% Mg-Al/$[Fe(CN)_6]$ LDH nanoadditive), one of the samples showed noticeably faster degradation compared to the plates with the reference coating (Figure 5A). This out-of-average result could be explained by the presence of coating defects, noticeable on visual analysis at the higher magnification (Figure 5B). The defects led to the diffusion of aggressive ions to the metal surface and, subsequently, faster degradation of the substrate. However, this example perfectly demonstrates the functionality of the sensing layer. The coating revealed blue spots with approximately the same diameter as the corrosion spots for the reference sample, after 8 h of immersion (Figure 5B). After 24 h of immersion (Figure 5A), the amount of tiny blue spots was massive and well-spread around the exposed area. Under magnification on the stereo microscope, some corrosion spots with diameters of 0.1–0.15 mm could already be found (Supplementary Figure S5). Quite interestingly, places that initially gave rise to larger blue spots (24 h and 48 h of immersion) turned into brownish precipitates for longer immersion times (72 h and 1 week of immersion) (Figure 5A).

Looking at the EIS spectra (Figures 5C–E), it is possible to observe that the impedance of the reference coating (Figure 5C) is the highest amidst the test systems, revealing a capacitive response throughout the whole immersion time (up to 1 week of immersion). Moreover, there is a decrease in the impedance at low frequencies of one order of magnitude within the first 24 h of immersion, though the impedance values remain quite high (~10^8 Ω cm^2) for the remaining immersion time. When the formulation is modified, either with LDH (Figure 5D), or the potassium salt (Figure 5E), the EIS spectra acquired after a few minutes of immersion reveal lower impedance magnitude at low frequencies with respect to the reference coating, and a resistive plateau can already be detected, that can be ascribed to the coating pore resistance. In addition, while the impedance magnitude of the LDH-based coating (Figure 5D) is similar to the coating with $K_3[Fe(CN)_6]$ (Figure 5E) right after immersion, the impedance of the former system decreases considerably within the first 24 h of immersion, with a second time constant being detected at low frequencies (ascribed to the corrosion processes). In the case of the coating with $K_3[Fe(CN)_6]$ (Figure 5E) the coating barrier properties are more stable throughout the immersion times and only the time constant associated with the coating can be detected.

As described above, the sample with 5 wt% Mg-Al/$[Fe(CN)_6]$ LDH presented in Figure 5D demonstrated the worst results of barrier properties among the measured samples with the same system due to the presence of coating defects. In other tested samples with 5 wt% LDH nanoadditive (Figure 6A) the decrease of the barrier properties was not so dramatic in comparison to the reference system (Figure 5C). These findings exemplify the lack of reproducibility of coating preparation and measurements, quite

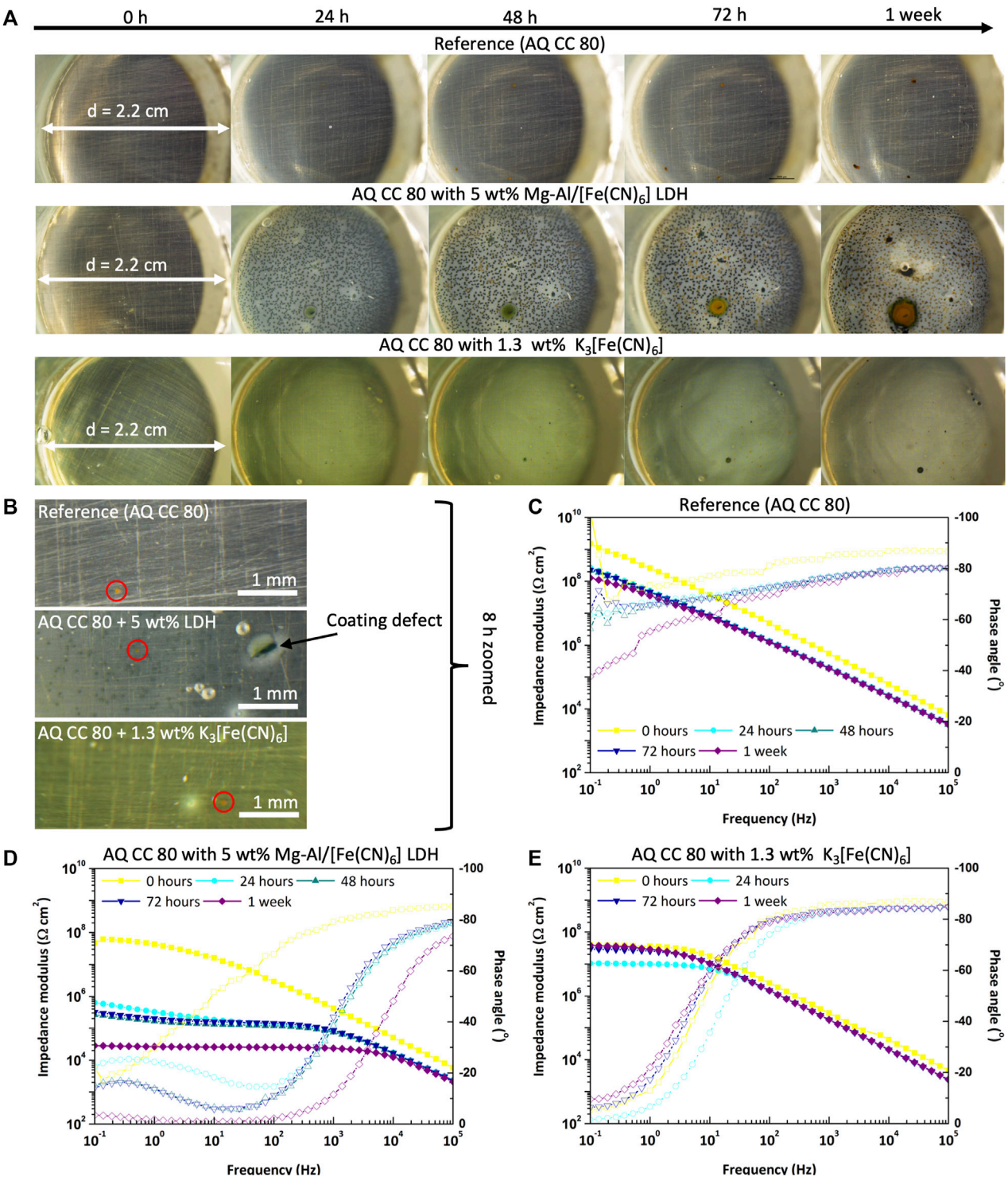

FIGURE 5
Visual analysis **(A, B)** and EIS plots **(C–E)** of carbon steel plates coated with acrylic polyurethane AQ CC 80 coating (reference) **(C)**, acrylic polyurethane AQ CC 80 coating with 5 wt% Mg-Al $[Fe(CN)_6]$ LDH nanoadditive (coating with a defect) **(D)**, and acrylic polyurethane AQ CC 80 coating with 1.3 wt% $K_3[Fe(CN)_6]$ additive **(E)**, immersed in 0.6 M NaCl during 1 week.

often not addressed in manuscripts. Moreover, even with a relatively small decrease in the impedance magnitude values, the corresponding colorimetric signal identifying the initiation of corrosion prosses was detected (Figure 6C), while Figures 5A, D clearly shows how the level of degradation correlates with the intensity of the colorimetric signal. Additionally, the coating with 10 wt% Mg-Al/$[Fe(CN)_6]$, subsequently tested, revealed the same trend (Figures 6B, D).

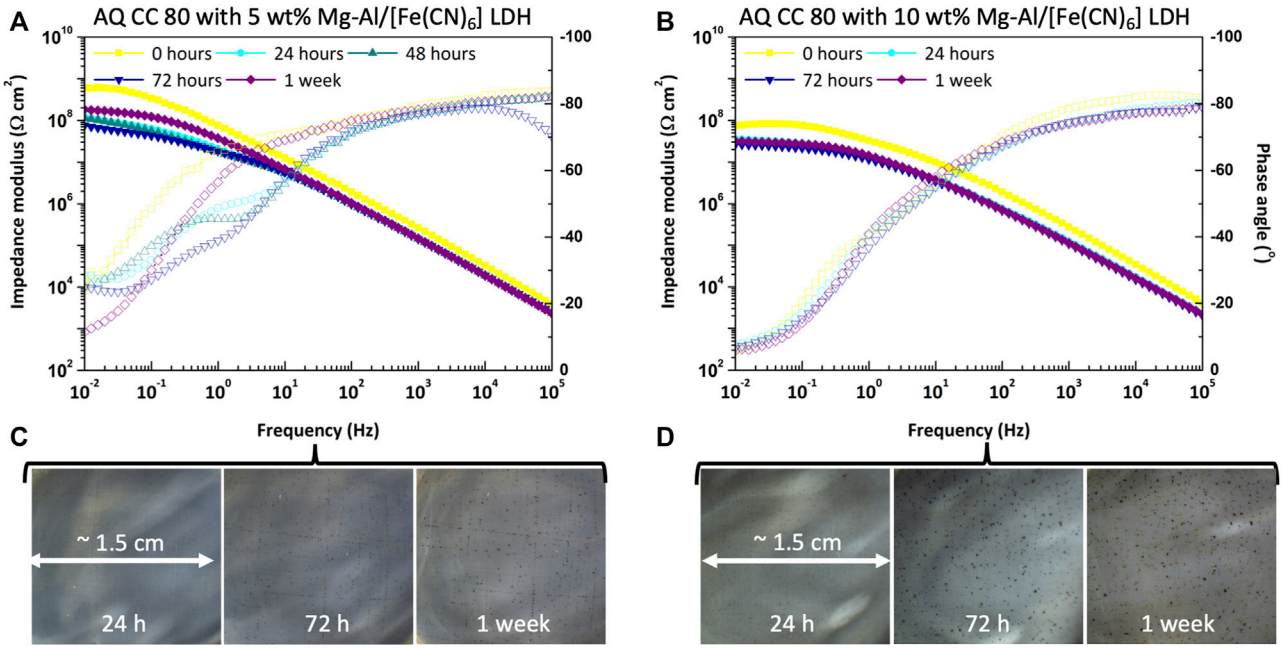

FIGURE 6
Study of corrosion of carbon steel plates coated with acrylic polyurethane AQ CC 80 coating with 5 wt% Mg-Al/$[Fe(CN)_6]$ LDH nanoadditive **(A, C)** and acrylic polyurethane AQ CC 80 coating with 10 wt% Mg-Al/$[Fe(CN)_6]$ LDH nanoadditive **(B, D)** immersed in 0.6 M NaCl during 1 week: EIS plots **(A, B)** and visual analysis **(C, D)**.

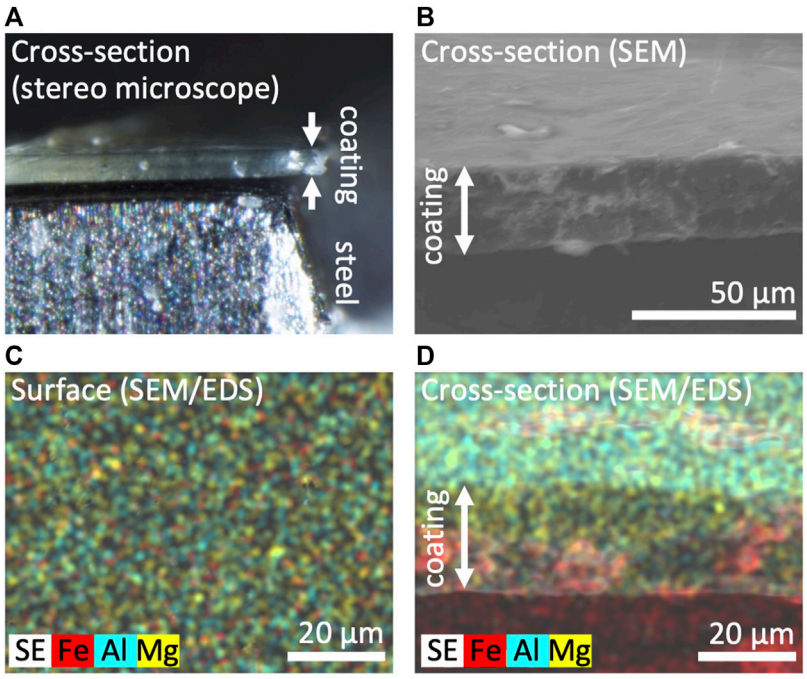

FIGURE 7
Analysis of the cross-section **(A, B, D)** and surface **(C)** of the acrylic polyurethane AQ CC 80 coating with 10 wt% Mg-Al/$[Fe(CN)_6]$ LDH sensing nanoadditive by stereo microscope **(A)** and SEM **(B)** and SEM/EDS mapping **(C, D)**.

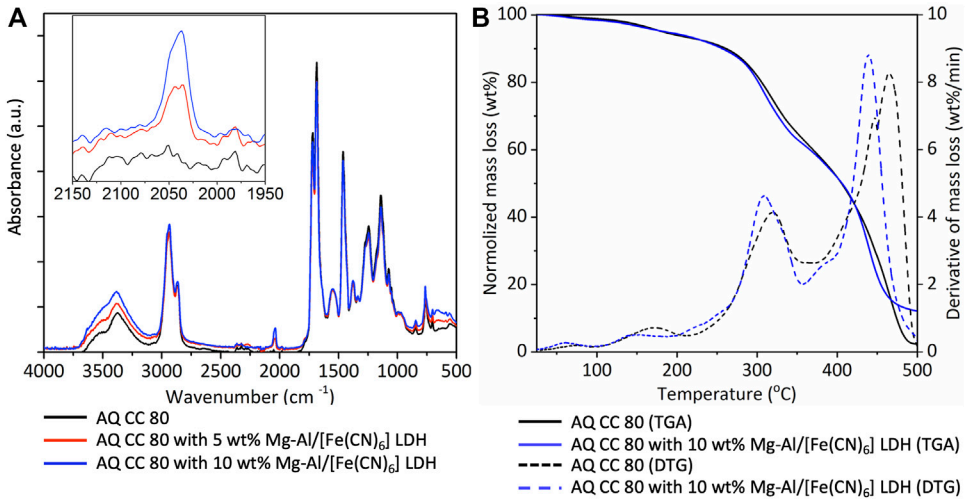

FIGURE 8
Structural characterization of acrylic polyurethane AQ CC 80 coating with and without Mg-Al/$[Fe(CN)_6]$ LDH nanoadditive via FTIR **(A)**, thermal characterization of acrylic polyurethane AQ CC 80 coating with and without Mg-Al/$[Fe(CN)_6]$ LDH nanoadditive via TGA and DTG **(B)**.

3.2.2.2 Morphology of the sensing layer

The analysis of the acrylic polyurethane AQ CC 80 coating with Mg-Al/$[Fe(CN)_6]$ LDH nanoadditive via stereo microscope (Figure 7A), SEM (Figure 7B), and SEM/EDS mapping (Figure 7C–surface; Figure 7D–cross-section) confirmed homogeneous dispersion of the LDH in the polymer. The presence of micro-scale aggregates was not detected. Both sensing and reference coatings showed smooth transparent surfaces, allowing to see the condition of the steel substrate under the film. It should be mentioned, that delamination of the coating at the edges of the plate, observed in Figure 7A, was probably caused by the deformation of the steel substrate during specimen preparation by guillotine cutting. Moreover, the apparent decrease of the coating thickness observed by SEM (Figures 7B, D) when compared to the use of coating thickness gauge, could be explained by variation of coating thickness in different parts of the relatively large sample prepared. The use of a bar coater applicator and the way the cured film may level in the edges of the sample with respect to the inner part of plate, may induce variations in coating thickness.

3.2.2.3 Structure of the sensing layer

The structure of the acrylic polyurethane AQ CC 80 coating with and without Mg-Al/$[Fe(CN)_6]$ LDH nanoadditive was characterized by FTIR spectroscopy (Figure 8A). The observed results are typical for a polyurethane coating (Trovati et al., 2010), showing intensive bands at 1,726, 2,935, and 2,864 cm^{-1} associated with carbonyl groups (Lewis et al., 1994; Trovati et al., 2010). The increase of a band near 3,400 cm^{-1} for the coatings with Mg-Al/$[Fe(CN)_6]$ LDH nanoadditive compared to the reference one can be associated with the stretching of the hydroxide groups and interlayer water molecules present in LDH (Kloprogge et al., 2002). Moreover, the appearance of a band at 2,036 cm^{-1} confirms the presence of hexacyanoferrate ion (Braterman et al., 1994). According to the data presented in the literature, the band associated with stretching of the CN group in hexacyanoferrate ion appears at 2,120–2,035 cm^{-1}, and its position depends on the oxidation state of iron (Hansen, 1994; Holgado et al., 1996). The appearance of the bands at 2,036 cm^{-1} is associated with the presence of $[Fe(CN)_6]^{4-}$ form, while a band characteristic for $[Fe(CN)_6]^{3-}$, which usually lies in the range at 2,120–2,086 cm^{-1} (Holgado et al., 1996), was not detected in the coatings.

3.2.2.4 Thermal stability and glass transition temperature of the sensing layer

The influence of the Mg-Al/$[Fe(CN)_6]$ LDH nanoadditive on the thermal stability of the acrylic polyurethane AQ CC 80 coating was evaluated via TGA and DTG, analyzing separated cured films (Figure 8B). Both the reference acrylic polyurethane AQ CC 80 coating and the coating with the sensing nanoadditive show good stability up to about 145°C. The addition of Mg-Al/$[Fe(CN)_6]$ LDH did not cause any significant influence on coating thermal stability in the tested concentration (10 wt%). At higher temperatures, the thermograms show two-step degradation with a significant increase in mass loss rate at about 240°C–320°C and about 390°C–460°C, indicating two-phase morphology, what is the expected behavior for an acrylic polyurethane polymer (Bahadur et al., 2016). Considering that the target application conditions of the sensing coating are well below the degradation temperatures, the nature of this process has not been further investigated in the frame of this work. After 500°C, the difference in the mass loss between the coating with the sensing additive and the reference coating was 9.8 wt%, which is consistent with the dry content of the nanoadditive.

The glass transition temperature (T_g) of the coatings was calculated from the DSC as half of C_p extrapolated using the equipment software (Supplementary Figure S6) and was found to be 38.18°C for the acrylic polyurethane AQ CC 80 coating without additives, and 45.16°C for the coating with 10 wt% Mg-Al/$[Fe(CN)_6]$ LDH nanoadditive.

TABLE 1 Vickers microhardness testing of the acrylic polyurethane coating with and without Mg-Al/[Fe(CN)$_6$] LDH nanoadditive (loading time 15 s).

Sample name	Hardness at different loads (kg_F/mm^2) ± SD		
	0.025 kg	0.050 kg	0.100 kg
AQ CC 80	4.3 ± 0.7	4.5 ± 0.3	5.0 ± 0.5
AQ CC 80 + 5 wt% LDH	15.2 ± 1.2	16.2 ± 0.6	17.1 ± 1.2

3.2.2.5 Influence of the sensing nanoadditive on coating mechanical properties

3.2.2.5.1 Adhesion tests. Adhesion tests were performed according to ASTM D3359. Observation of the tested areas confirmed that the addition of Mg-Al/[Fe(CN)$_6$] LDH nanoadditive did not cause changes in the coating adhesion in the range of concentrations tested (5 and 10 wt%), with all the samples showing good adhesion to the steel substrate (Supplementary Figure S7). No flaking was detected on the surface of the cross-cut area, all the edges of the cuts were completely smooth, and none of the squares of the lattice was detached, which corresponds to the best test results (5B) according to the ASTM D3359 classification table (ASTM, 2022).

3.2.2.5.2 Hardness tests. To investigate the ability of the developed sensing layer to resist plastic deformation, the hardness of the acrylic polyurethane AQ CC 80 coating with 5 wt% Mg-Al/[Fe(CN)$_6$] LDH nanoadditive and of the reference coating (without additive) applied on steel substrates were evaluated by the micro Vickers hardness method applying various loads during 15 s. The resulting indentations were analyzed using the stereo microscope. The hardness was calculated as the ratio of load and surface area of the resulting pyramidal impression (Wu et al., 2022) (4):

$$HV = \frac{F}{A} = \frac{F}{d^2 / \left(2 \sin \frac{\alpha}{2}\right)} \approx 0.1891 \frac{F}{d^2} \quad (4)$$

where HV is the hardness of the material in kg_F/mm^2, F is the force applied to the diamond in kg_F, A is the surface area of the resulting indentation in mm^2, α is the mean angle between the opposite faces at the vertex of the pyramidal indenter ($\alpha = 136^\circ$), and d is the average length of the two diagonals left by the indenter in mm.

Despite the viscoelastic behavior of the polymer (elastic deformation under the load followed by viscoelastic flow after unloading), the elastic recovery in the direction of the diagonals of the indentation is usually inappreciable (Low and Shi, 1998). Therefore, the measurement of the lengths of the diagonals should give reliable hardness for the studied polymeric coatings. The obtained HV values are consistent in the range of the tested loads (Table 1). A minor increase in the hardness of the samples is observed with the increase of the applied force. Addition of 5 wt% Mg-Al/[Fe(CN)$_6$] LDH nanoadditive has a positive effect on the coating hardness, increasing it by 3.5 times (Table 1), reflecting a higher resistance to scratching and to mechanical damage of the resulting composite coating. The obtained values lie in the range typical for polymeric materials and their composites (Galvão et al., 2018; Wu et al., 2022).

3.3 Multilayer protective coating systems

3.3.1 Preparation of the multilayer coating systems

The main goal on the basis of the development of a sensing layer to detect corrosion of metallic substrates is to test and validate it in conditions observed during the service life of exposed structures, such as in offshore conditions. As a result, and considering that the sensing layers do not provide a long-lasting protective effect in terms of corrosion, it was decided to develop a multilayer system, with the sensing layer described in previous sections, applied directly onto the metal substrate, followed by the application of an additional topcoat without the LDH nanoadditive to enhance barrier against the ingress of aggressive species when exposed to harsh conditions. Thus, the sensing layer for color detection was based on the acrylic polyurethane AQ CC 80 coating described earlier, whilst several commercial coatings were studied as possible topcoats, among which a solvent-based transparent epoxy varnish and a solvent-based transparent polyurethane were ultimately selected. The selection criteria for a topcoat were: good adhesion to the organic coating sensing layer, high barrier properties, and transparency of the coating. The system with the epoxy-based topcoat is referred hereafter as *multilayer system 1*, and the system with the polyurethane-based topcoat as the *multilayer system 2* (Supplementary Table S1).

3.3.2 Corrosion sensing and corrosion protection performance of the multilayer coating systems

The corrosion sensing and corrosion protection performance of the prepared multilayer coating systems were first investigated at lab scale by following the corrosion of the coated steel plates immersed in 0.6 M NaCl solution via EIS measurements and optical analysis of the surface. The coatings systems with the Mg-Al/[Fe(CN)$_6$] LDH sensitive nanoadditive were compared to the corresponding reference multilayer systems (without the LDH nanoadditive). The dry thickness, measured by the coating thickness gauge, was found to be about 70 ± 10 µm for the *multilayer system 1* with the epoxy topcoat and about 50 ± 10 µm for the *multilayer system 2* with the polyurethane topcoat.

In the case of the *multilayer system 1* with the epoxy topcoat (Figure 9), the visual analysis of the immersed coated steel plates (Figure 9A) showed that the reference multilayer system remained transparent throughout the immersion period sampled (up to 1 week of immersion). Small corrosion spots invisible to the naked eye were detected under the stereo microscope (×4 magnification) after 1 week of immersion. At the same time, in the samples with the Mg-Al/[Fe(CN)$_6$] LDH sensing nanoadditive, after 1 week of immersion, it is possible to see the occurrence of several small blue spots indicating the initiation of the corrosion process (Figure 9A). Regarding the analysis of EIS spectra,

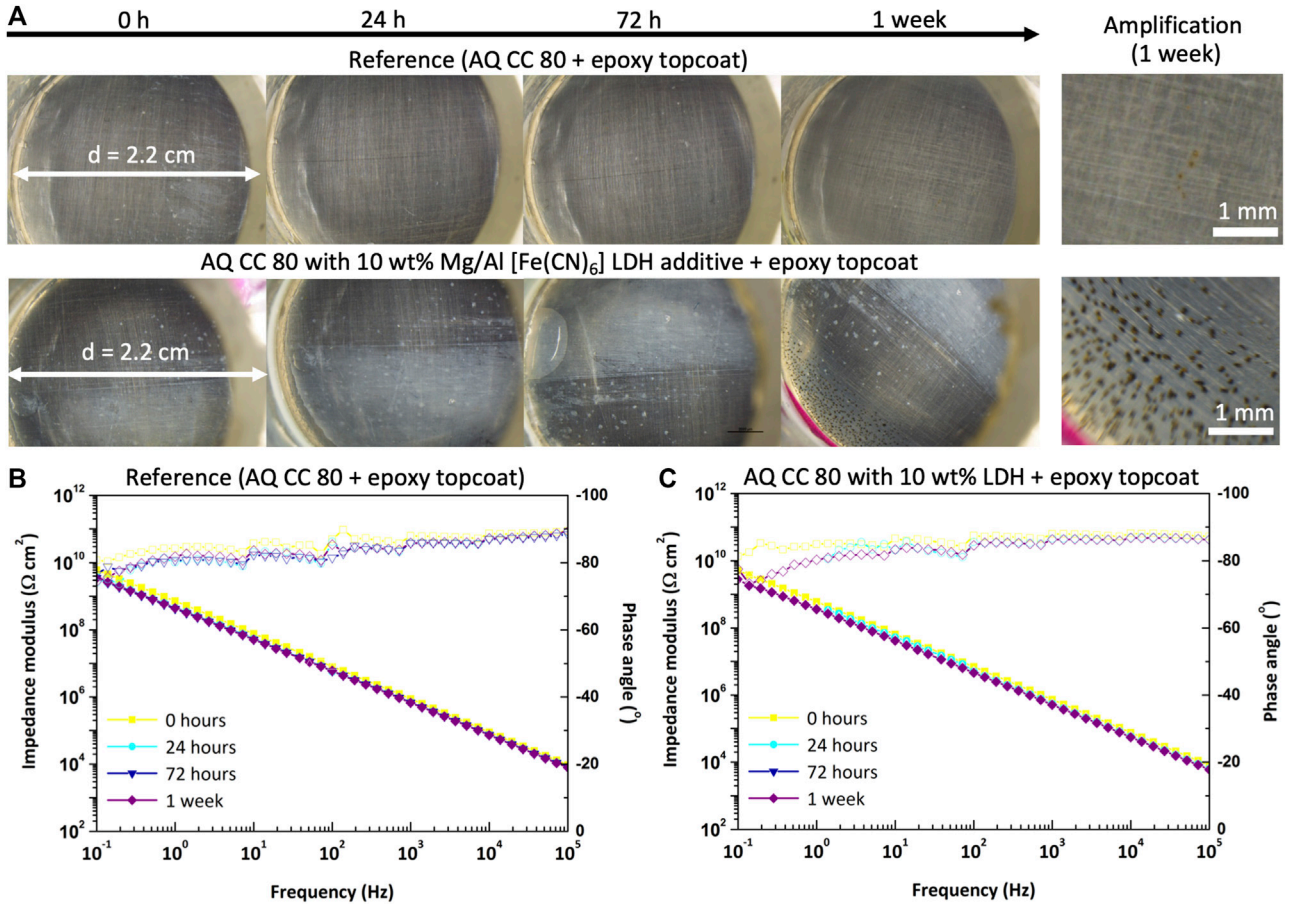

FIGURE 9
Visual analysis of the surface **(A)** and EIS spectra **(B, C)** of carbon steel plates coated with the *multilayer system 1* with Mg-Al/[Fe(CN)$_6$] LDH nanoadditive **(C)** and corresponding reference multilayer system without the additive **(B)** immersed in 0.6 M NaCl solution during 1 week.

it is possible to observe that both *multilayer system 1* with the sensing nanoadditive (Figure 9C) and the corresponding reference multilayer system (Figure 9B) show a capacitive behavior, with low-frequency impedance magnitude values being in the GΩ cm^2 range, throughout the sampled time (up to 1 week of immersion).

The *multilayer system 2* with the polyurethane topcoat (Figure 10) also shows the improvement of the barrier properties (Figure 10C) with respect to the single-layer sensing coating based on AQ CC 80 (Figure 5D). Nonetheless, the barrier properties of this system decreased markedly within the first 1—2 days of immersion (Figure 10C). This can be inferred from the visual inspection of the samples in Figure 10A with the occurrence of very barely visible blue spots on the coating with the LDH nanoadditive after 24 h of immersion (zoomed image of the surface after 24 h is provided in the Supplementary Figure S8), which becomes more intense after 48 h. At the same time, corrosion spots invisible to the naked eye were detected at the corresponding reference coating using the stereo microscope with ×4 magnification (Figure 10A; Supplementary Figure S8). The results of the optical analysis are consistent with the EIS data (Figure 10B), where a well-defined resistive plateau in the low-frequency range can be observed. One time constant associated with the coating response is detected throughout the immersion times monitored, although for the LDH-containing coating the appearance of one additional time constant at low frequencies after 48 h of immersion (Figure 10C) can be associated with ongoing corrosion processes at the metal substrate. Overall, *multilayer system 2* shows a faster degradation when compared to *multilayer system 1*.

3.3.3 Structure and morphology of the multilayer systems

The adhesion of the multilayer systems to the steel substrate was tested according to ASTM D3359. Observation of the tested areas confirmed that both multilayer systems showed good adhesion, corresponding to the best test results (5B) according to the ASTM D3359 classification table (ASTM, 2022), and the addition of the sensing nanoadditive does not influence the coating performance. On the surface of the section of the transverse cut, no delamination was detected, all the edges of the cuts were completely smooth, and none of the squares was peeled off (Supplementary Figure S9).

The structure and morphology of the coating systems were investigated via stereo microscopy and SEM/EDS. All systems showed smooth uniform surfaces. The coatings were colorless

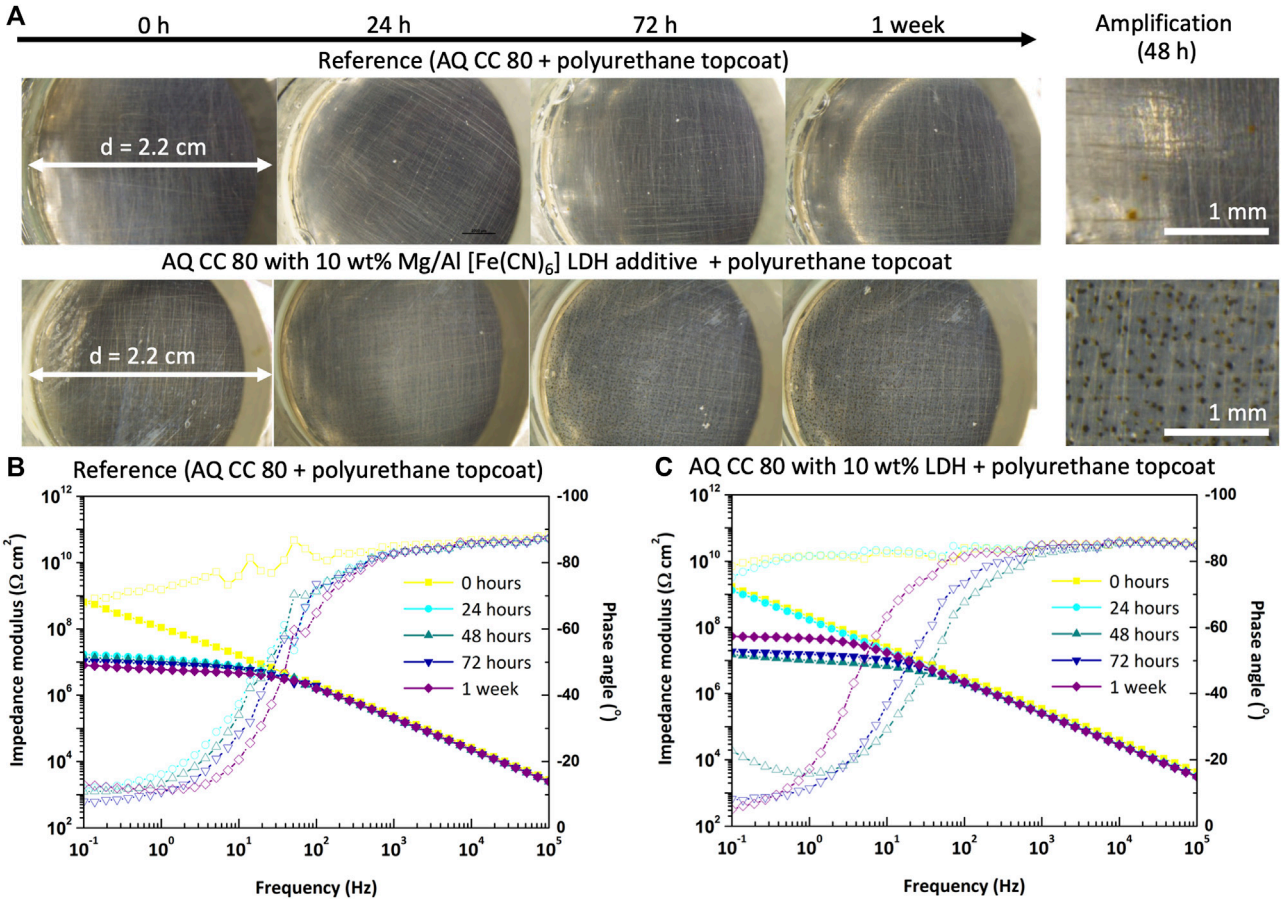

FIGURE 10
Visual analysis of the surface **(A)** and EIS spectra **(B, C)** of carbon steel plates coated with the *multilayer system 2* with Mg-Al/$[Fe(CN)_6]$ LDH nanoadditive **(C)**, and corresponding reference multilayer system **(B)** immersed in 0.6 M NaCl solution during 1 week.

and transparent, allowing good observation of the substrate. Samples prepared after 1 week of immersion in 0.6 M NaCl solution revealed swelling of the coatings, with the resulting thickness of the multilayer system 2 being around 70 ± 10 µm, while in the case of the multilayer system 1 the thickness was in the range of 100 ± 20 µm. SEM analysis of the films detached from the substrate (Figures 11A, C) revealed a smooth connection between the two organic layers in both multilayer systems. EDS mapping (Figures 11B, D) allows seeing the location of the layer border (the concentration of Mg and Al is higher in the sensing layer due to the presence of Mg-Al LDH).

3.4 Validation of corrosion detection functionality by standard testing

As both multilayer systems were found to be stable and relevant for further studies, the corrosion-protective performance and the sensing functionality of both systems were further investigated by the standardized salt spray test according to ISO 9227 (ISO and CEN, 2022) to validate the results from the lab scale immersion tests. For this purpose, steel plates coated with the multilayer coating systems were exposed to the salt fog that mimics natural weather conditions. The backside of the plates was covered with a thick layer of epoxy to protect it from corrosion. The edges of the plates were additionally covered with a varnish. Samples retrieved from the salt spray chamber were analyzed visually to follow the effects associated with the corrosion process (Figure 12).

The *multilayer system 1* containing the LDH sensing non-additive revealed the signal associated with early-stage corrosion of steel plates already after 48 h of salt spray testing. More specifically, several pale blue dots were detected near the edges of the plates (Figure 12), which implies that the protective measures used to isolate the faces may have not been as effective as initially expected. During the following days in the salt spray chamber, the signal intensifies a little bit, and additional dots appeared near the edges. No traces of brownish corrosion products were observed in the center of the plates, confirming the good barrier properties of the coating itself. The corresponding reference coating (without the LDH nanoadditive) revealed no visible signs of corrosion in the center but an accumulation of brown corrosion products in the varnish protecting the edges (Supplementary Figure S10). In the *multilayer system 2,* corrosion of the steel substrates occurred faster. The coating with the sensing nanoadditive revealed blue spots already after 24 h of salt spray exposure. The signal was more intense and covered bigger parts of the surface when

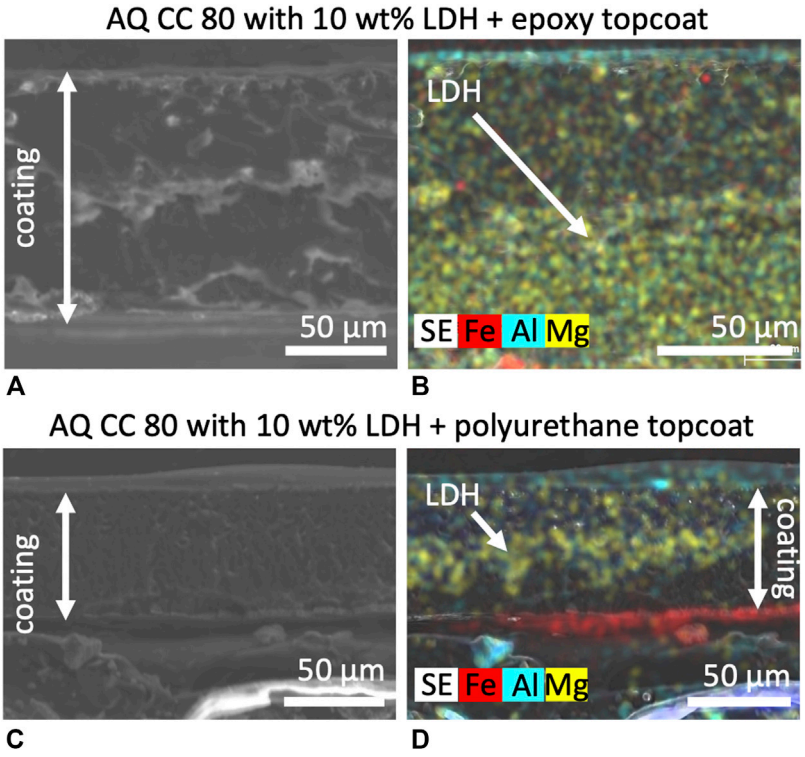

FIGURE 11
SEM imaging **(A, C)** and EDS mapping **(B, D)** of the multilayer coating systems with Mg-Al/$[Fe(CN)_6]$ LDH sensing nanoadditive: *multilayer system 1* **(A, B)** and *multilayer system 2* **(C, D)**.

compared to *multilayer system 1*, indicating a higher level of degradation (Figure 12). The color of the blue spots intensified during salt spray exposure. Overall, the salt spray test results confirmed the immersion test results obtained at lab scale.

4 Discussion

4.1 Previous work and novelty

The use of active nanoadditives, able to react with species generated during the corrosion process giving a visual colorimetric signal, to produce "smart" corrosion sensing coating is not a new idea. However, despite the recent progress in the self-reporting coatings (Bouali et al., 2020; Ma et al., 2021; Chen et al., 2023), the development of environmentally friendly solutions acceptable for offshore applications is a relevant issue. Some of the coatings reported in the literature, whose detection mechanism is based on sensing the pH change associated with the beginning of the corrosion process, (Wang et al., 2018; Liu et al., 2020), could meet challenges in the sea environment due to the high pH of the seawater. In other cases, the detection mechanism reported is based on the reaction of iron cations with indicating species (G.S. Dhole et al., 2015; Lv, et al., 2021b; Taheri et al., 2022) that can exhibit high toxicity towards marine organisms (Feldmannová et al., 2006; Yan et al., 2015; Skjolding et al., 2021), so their use in offshore environments may pose additional challenges. Our previous work (Wilhelm et al., 2020) was dedicated to the development of an environmentally friendly sensing additive able to detect early-stage corrosion on a carbon steel substrate, and hexacyanoferrate intercalated LDH were proposed as a promising material. The work was focused on the selection of the most appropriate LDH composition, study of precursor materials, and testing of the developed sensing additive in model solutions under conditions relevant to the corrosion process. Mg-Al/$[Fe(CN)_6]$ LDH were found to detect corrosion processes on uncoated carbon steel, demonstrating the controlled release of the active anion under corrosive conditions. The environmental behavior of the developed nanoadditive in saltwater and the effect of the 'nanosensor' and its components on the marine microalgae is demonstrated in our recently published paper (Martins et al., 2022).

The present work is devoted to: 1) the development of a sensing coating with Mg-Al/$[Fe(CN)_6]$ LDH nanoadditive; 2) investigation of compatibility of the sensing nanoadditive with commercial coating formulation based on water-based acrylic urethane; 3) testing of corrosion protection and early-stage corrosion detection functionality of the developed sensing coating on carbon steel substrate; and 4) subsequent development of a multilayer system with additional protective topcoat for improvement of barrier properties of the sensing coating. Two topcoats based on different chemistries were examined in the frame of this work as a possible solution for the protective layer in the multilayer system. The results on corrosion protection performance and corrosion sensing functionality were verified by salt spray tests. As far as we

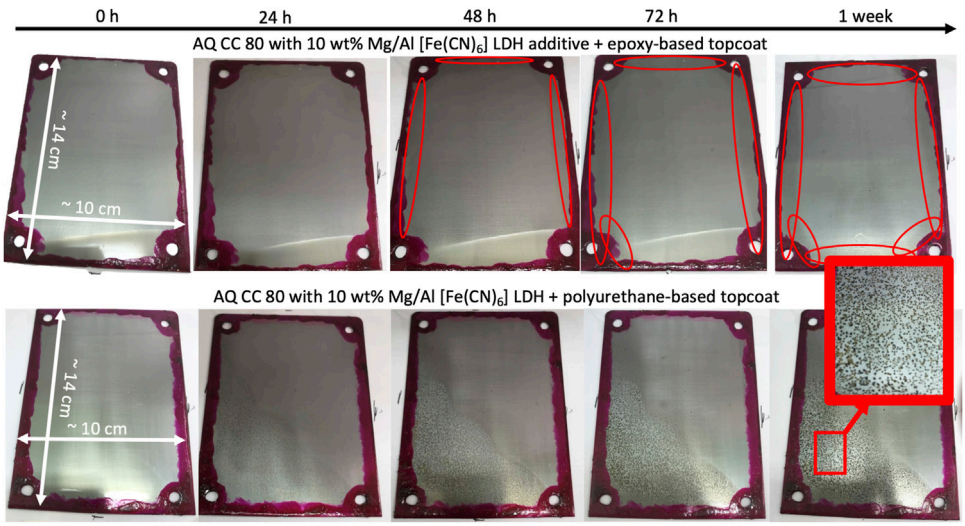

FIGURE 12
Salt spray test results for the carbon steel plates coated with multilayer coating systems with 10 wt% Mg-Al/[Fe(CN)$_6$] LDH sensing nanoadditive.

know, no studies on corrosion sensing coating based on hexacyanoferrate intercalated LDH nanoadditive have been reported in the literature.

4.2 Compatibility of the Mg-Al/[Fe(CN)$_6$] LDH sensing nanoadditive with the acrylic polyurethane coating

The Mg-Al/[Fe(CN)$_6$] LDH sensing nanoadditive showed good compatibility with the acrylic urethane coating formulation in the tested concentration range up to 10 wt%. The ultrasound treatment allowed to achieve a homogeneous distribution of the nanoadditive without any visual aggregation, which was subsequently confirmed by the stereo microscope as well as by investigation of cured coating cross-sections via SEM/EDS (Figure 7).

Functionality tests of coating formulations with Mg-Al/[Fe(CN)$_6$] LDH confirmed that the coating formulation components did not influence the ability of the hexacyanoferrate ion to detect iron cations (Figure 2). The observed initial lower signal intensity in formulation with Mg-Al/[Fe(CN)$_6$] LDH nanoadditive in comparison to the formulation with hexacyanoferrate directly dispersed in solution, and subsequent signal intensification of the former one, could be associated with the gradual release of the active anion from the LDH nanocarriers. The mechanism of release of hexacyanoferrate anion from Mg-Al LDH was described in detail in our previous work (Wilhelm et al., 2020). In outline, LDH are able to respond to the conditions relevant to the corrosion process, releasing the active anion via an ion-exchange process. The controlled release of the active agent from the nanocarriers was previously shown to prolong the action of the additive and to allow a reduction of toxicity (Martins et al., 2022). Furthermore, the positive effect of the implementation of active agents in LDH for application in protective coatings was demonstrated by many researchers for different materials (Poznyak et al., 2009; Tedim et al., 2012; Sui et al., 2022). The use of LDH is especially relevant for offshore applications, where the presence of chloride ions is typical in the environment: after penetration through the coating, chloride ions enable the release of the active anion from LDH through the ion-exchange mechanism, allowing the detection of the initiation of corrosion processes (Bouali et al., 2020).

In the present work, the compatibility of the Mg-Al/[Fe(CN)$_6$] LDH with the water-based acrylic urethane AQ CC 80 coating formulation was also investigated by rheological studies. The addition of the LDH did not show any negative effect on the coating formulation in the range of tested concentrations (Figure 3). Moreover, as expected for a LDH nanoadditive (Basu et al., 2014), it has a positive effect on the mechanical properties of the cured coating, increasing its hardness, which could increase coating resistance to scratches and mechanical damage. The coating properties analyzed herein are in agreement with data published in the literature for polyurethane coatings (Trovati et al., 2010; Galvão et al., 2018).

The developed sensing layer showed good thermal stability up to 145°C. Incorporation of the Mg-Al/[Fe(CN)$_6$] LDH nanoadditive (10 wt%) increases the glass transition temperature of the coating in 6.98°C, (T_g = 45.16°C). The increase of the T_g upon the incorporation of the LDH agrees with other studies of polyurethane/LDH composites presented in the literature (Yu et al., 2014; Moshkriz and Darvishi, 2022), and could be associated with an interaction of nanoparticles with polymer chains, thereby limiting the mobility of the latter near polymer/LDH interface (Yu et al., 2014). The T_g of the sensing layer allows its curing at a relatively low temperature, which is important for large-scale applications, wherein it is high enough to ensure a hard (glassy) state of the coating at room temperature providing appropriate mechanical properties.

An important point coming out from the results of compatibility testing is a reduction of hexacyanoferrate anion

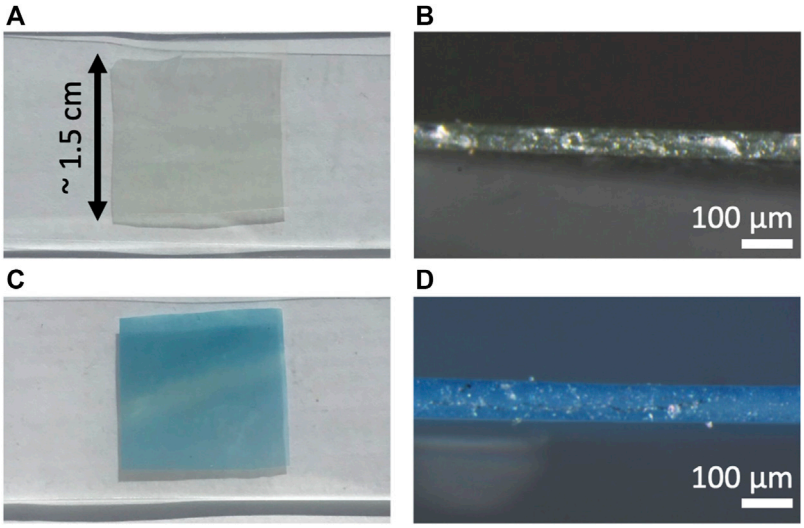

FIGURE 13
Acrylic polyurethane AQ CC 80 coating with 5 wt% Mg-Al/$[Fe(CN)_6]$ LDH sensing nanoadditive before **(A, B)** and after **(C, D)** immersion in Fe(III) salt solution: top view **(A, C)** and analysis of the cross-section on the stereo microscope at ×13.5 magnification **(B, D)**.

from $[Fe(CN)_6]^{3-}$ to the $[Fe(CN)_6]^{4-}$ form inside the cured acrylic polyurethane coating (Figure 8A). However, it was shown that both forms of the hexacyanoferrate anion are able to react with Fe cations, giving rise to blue precipitates (Weiser et al., 1942; Wilde et al., 1970) (5, 6):

$$4Fe^{3+}_{(aq)} + 3[Fe(CN)_6]^{4-}_{(aq)} \leftrightarrow Fe_4[Fe(CN)_6]_{3\,(s)} \quad (5)$$

$$3Fe^{2+}_{(aq)} + 2[Fe(CN)_6]^{3-}_{(aq)} \leftrightarrow Fe_3[Fe(CN)_6]_{2\,(s)} \quad (6)$$

To prove this claim, coating films of AQ CC 80 with 5 wt% LDH sensing nanoadditive were tested by exposing the coating films to Fe^{2+} and Fe^{3+} containing aqueous solutions for 24 h. Iron (II) chloride tetrahydrate and iron (III) nitrate nonahydrate were used as sources of Fe^{2+} and Fe^{3+} cations, respectively. Immersion in iron (II) aqueous solution did not give rise to the blue colorimetric response, while a strong reaction could be observed with the iron (III) salt (Figures 13A, C), confirming the FTIR results described before. The coloration is intense and uniform throughout the entire thickness of the coating (Figure 13D). After immersion, swelling of the coating and an increase in coating thickness was observed as well (Figures 13B, D). Therefore, the detection mechanism of the developed sensing coating is mainly based on the reaction with Fe^{3+} cations (reaction 5), generated during the steel corrosion process due to the oxidation of Fe^{2+} to Fe^{3+}. Nevertheless, one cannot completely rule out the formation of blue precipitates as described in reaction 6 directly from Fe^{2+}, as this is the one iron species to be formed first, and because these reactions are not complete but rather governed by a chemical equilibrium, which can shift directions depending on the relative concentration of the involved species. According to the data published in the literature (Weiser et al., 1942), the following reaction could take place during the corrosion process upon mixing of hexacyanoferrate ions with ferric cations:

$$Fe^{3+} + [Fe^{2+}(CN)_6]^{4-} \rightarrow Fe^{2+} + [Fe^{3+}(CN)_6]^{3-} \rightarrow Fe^{2+}_3[Fe^{3+}(CN)_6]^{3-}_2 \downarrow \quad (7)$$

4.3 Corrosion detection and corrosion protection performance of the sensing layer

Considering the visual inspection of samples exposed to 0.6 M NaCl solution during the EIS measurements, three main points can be highlighted (Figures 5, 6):

- First, it seems that corrosion proceeds slightly faster in the coating with the LDH. It is well known that often the addition of inorganic particles to a polymer-based model formulation can result in a partial decrease of the barrier properties because the formulations were not optimized in terms of pigment and filler content at this basic level of research. This is an aspect that, from an industrial perspective, can be circumvented in terms of coating development. Several examples showing the negative effect of adding particles to model formulations can be found in the literature, including in other works from our group (Maia et al., 2012). Another factor not considered is the coating thickness: the operators controlled only the coating wet thickness during the application process, not the final drying thickness, and lower barrier properties can also be due to the lower coating dry thickness.
-Second, the blue spots appeared always first than corrosion products, meaning that Mg-Al/$[Fe(CN)_6]$ LDH nanoadditive, indeed allows the detection of oxidized iron cations *before* the precipitation of corrosion products occurs. Neither signs of corrosion nor appearance of colorimetric signals associated with formation of Prussian/Turnbull's Blue were detected before the immersion of the steel plates in a corrosion accelerating environment, as well as on the plates stored in ambient conditions in the laboratory throughout all the testing periods.

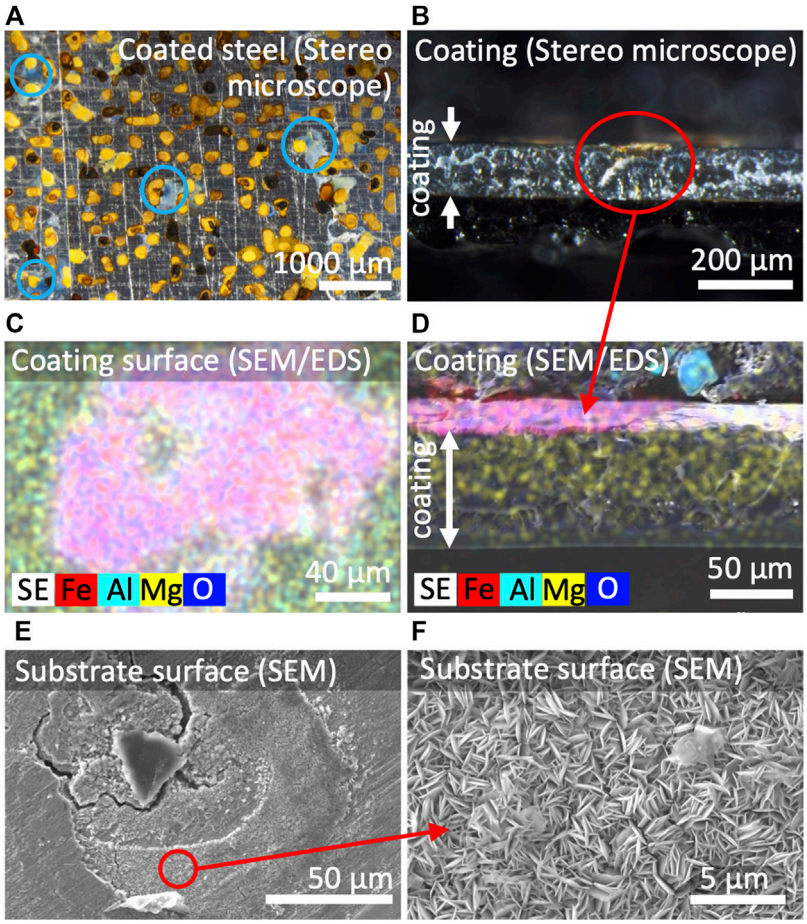

FIGURE 14
Analysis of the surface of corroded coated with *multilayer system 2* carbon steel plate via the stereo microscope **(A)**, analysis of the cross-section of its separated coating (metal-coating interface side is faced to the top) via the stereo microscope **(B)**, SEM/EDS analysis of the surface of the separated coating from the metal-coating interface side **(C)** and SEM/EDS analysis of the cross-section of the separated coating (metal-coating interface side is faced to the top) **(D)**, and analysis of the steel substrate after removal of the coating via SEM at the magnification ×800 **(E)**, ×6,000 **(F)**.

Moreover, no color change was detected on the separated coating films even after 1 week immersion in the corrosive environment (0.6 M NaCl). These observations support the assumption that the observed blue colorimetric signal on the coated steel plates is associated with the corrosion of the substrate caused by exposure to an external aggressive environment.

-The third point is that implementation of hexacyanoferrate ion in LDH significantly improves the detection functionality compared to the hexacyanoferrate dispersed directly in the coating, which gave very weak signals or no signal at all, while corrosion was already becoming evident.

4.4 Limitations and potential for application

The main limitation of the developed sensing layer, as was discussed above, is the negative effect of the LDH nanoadditive on the barrier properties of the coating. The results obtained from testing of the multilayer systems by EIS demonstrated that the addition of a protective topcoat without the LDH additive allows to overcome this limitation. The approach using a multilayer coating opens a possibility of modeling systems with different properties depending on the targeted functionalities and operating conditions by varying coating chemistry and thickness of the topcoat.

Both studied multilayer systems showed improvement in barrier properties compared to the single-layer system, without affecting the corrosion detection functionality. An important output of the corrosion studies of the multilayer system is that while *multilayer system 2* (with polyurethane topcoat) shows a correlation between the visual detection of blue spots and a marked decrease of barrier properties inferred from the EIS spectra, *multilayer system 1* (with the epoxy topcoat) brings one additional aspect to the discussion: in highly capacitive systems, where only water may diffuse (Yang et al., 2020), corrosion can occur at the metal surface but not be detected electrochemically (if the flow of ions across the coating is not significant). In this case, the use of additional corrosion sensors is of utmost importance since the electrochemical measurements do not reveal marked changes in the coating system.

Another limitation that has been noticed in some of the samples, is the change of the "signal" color over time. Examining the samples

a few weeks after salt spray tests revealed that part of the blue dots that were observed on the coating earlier turned to yellow or orange. To understand the ongoing process, a corroded carbon steel plate coated with *multilayer system 2* was investigated, when most of the blue dots, associated with the formation of Prussian/Turnbull's Blue, turned yellow (Figure 14A). For this purpose, the coating was detached from the corroded substrate and analyzed via stereo microscope (Figure 14B), SEM, and SEM/EDS (Figures 14C, D; Supplementary Figure S11) as well as the metal surface under the coatings (Figures 14E, F; Supplementary Figure S12).

This analysis revealed that yellow-to-brownish deposits are formed predominantly at the metal-coating interface (Figures 14B, D), while blue coloration, associated with the formation of Prussian/Turnbull's Blue, still can be observed across the coating thickness (Figure 14A). A more detailed study of the substrate surface (Figures 14E, F) and the surface of the separated coating from the metal-coating interface side (Figure 14C) via SEM and SEM/EDS, revealed the platelet structure of the deposits with an average particle diameter of around 1.5 nm and thickness of less than 0.01 nm. EDS analysis confirmed the presence of components of the sensing nanoadditive (Mg and Al) in the coating (Figures 14C, D) and at the substrate surface after the coating removal (Supplementary Figure S12). However, the observed yellow-to-brownish deposits mainly consisted of iron and oxygen (Figures 14C, D), which is consistent with the chemical composition of iron-based corrosion products. A possible explanation for this change, from the initial blue spots to the yellow-to-brownish ones, is a reaction that could take place on the metal-coating interface after long-term corrosion processes. More specifically, Prussian Blue could react with hydroxide ions generated during corrosion leading to the formation of iron hydroxide (III) (Noël et al., 2016) (8):

$$Fe_4^{3+}\left[Fe^{2+}(CN)_6\right]_3 + 12\,OH^- \rightarrow 4Fe(OH)_3 + 3\left[Fe^{2+}(CN)_6\right]^{4-} \quad (8)$$

To confirm that the seawater environment does not react with Prussian/Turnbull's blue formed inside the coating layer, samples of "blue" acrylic polyurethane AQ CC 80 film with 5 wt% Mg-Al/[Fe(CN)$_6$] LDH sensing additive (i.e., after reaction with Fe cations solution) were immersed in solutions with artificial seawater (ASW) with pH 8.0, NaOH solution with pH 9.0, and NaOH solution with pH 11.0. Photos of the films after 1 week of immersion are presented in Supplementary Figure S13. ASW was prepared using Pro-Reef meersalz/sea salt (Tropic Marin) according to the manufacturer's instructions. The films immersed in the ASW and NaOH solution with pH 9.0 did not show any visible change in the colorimetric signal, both films remained bright blue throughout the test period (2 weeks), while the film immersed in NaOH solution with pH 11.0 gradually discolored, and after 1 week of immersion became colorless. Upon re-immersion of the discolored film in solution with Fe^{3+} cations the blue color becomes visible after about 24 h of immersion, though less intense than in the beginning of the experiment (Supplementary Figure S13E). To confirm that the seawater environment will not interfere on the detection mechanism of the sensing layer, another test was performed by immersion of samples of acrylic polyurethane AQ CC 80 film with 10 wt% Mg-Al/[Fe(CN)$_6$] LDH in ASW with Fe^{2+} and ASW with Fe^{3+} cations, and pH 9 buffer solutions with Fe^{2+} and Fe^{3+} cations. In both ASW and buffer solution environments a bright blue signal across coating thickness was observed in solution with Fe^{3+} and a light blue color was detected in solutions with Fe^{2+} cations (Supplementary Figure S14). As mentioned above, the average pH of the ocean surface is 8.1, with the maximum at about pH 9.0 (Halevy and Bachan, 2017). Therefore, it can be concluded that the seawater environment neither interfere with the sensing mechanism of the developed coating nor react with Prussian/Turnbull's blue formed inside the sensing layer.

A long-term study of the coating barrier properties and corrosion sensing functionality is required for a better understanding of the coating performance and is currently in the process. Another important aspect to be considered is that the sensing coating system should be tested in the presence of other pigments to investigate the masking effect on the colorimetric signal. This is a study currently being carried out, together with the improvement of the coating barrier properties.

5 Conclusion

In this work, novel composite functional coating systems for carbon steel, able to detect corrosion at an early stage, were developed. Environmentally friendly Mg-Al/[Fe(CN)$_6$] LDH sensing nanoadditive able to detect iron cations generated during corrosion processes, was incorporated into a water-based acrylic polyurethane coating. The nanoadditive showed good compatibility with the coating formulation in the range of the concentrations tested. No negative effect of the nanoadditive on the viscous and viscoelastic behavior of the coating formulation has been found. Moreover, Mg-Al/[Fe(CN)$_6$] LDH additive showed a positive influence on the coating's mechanical properties by increasing its hardness, which can improve the resistance to scratching and mechanical damage. A systematic study of carbon steel plates coated with the developed sensing coating and immersed in an aggressive corrosion environment relevant for offshore application, was performed via electrochemical and visual monitoring of the system during the corrosion process to correlate the level of degradation of the substrate and the corresponding colorimetric signal. Successful detection of early-stage corrosion by revealing a blue color, associated with Prussian/Turnbull's Blue, was confirmed. Furthermore, the decrease in the coating barrier properties induced by the LDH nanoadditive was overcome by the development of a multilayer system with the implementation of an additional protective layer without the LDH additive, with salt spray testing validating the corrosion detection functionality investigated prior at a lab scale. Two topcoats with different chemistries (epoxy- and polyurethane-based) were tested as the protective layer in the multilayer system. Both multilayer coating systems are able to detect early-stage corrosion of carbon steel substrate although the multilayer coating system with the epoxy-based topcoat showed the highest barrier properties among the studied systems.

Data availability statement

The raw data supporting the conclusion of this article will be made available by the authors, without undue reservation.

Author contributions

AS is the first author, contributed to the main experimental work activities, performed data processing, and analysis of results, and drafted and wrote the manuscript in consultation with JT. RM and TP contributed for the main experimental work activities. IS performed a part of the experimental work. CN and MF contributed equally for the discussion and revision of the manuscript. JT is the senior and last author, designed the main experimental work, provided supervision of the work and project coordination, and is one of the main contributors for the writing of the paper. All authors contributed to the article and approved the submitted version.

Funding

The work was developed in the frame of the SMARTAQUA project, funded by the Foundation for Science and Technology in Portugal (FCT), the Research Council of Norway (RCN-284002), Malta Council for Science and Technology (MCST), and co-funded by European Union's Horizon 2020 research and innovation program under the framework of ERA-NET Cofund MarTERA (Maritime and Marine Technologies for a new Era), and in the scope of a COAT4LIFE project under Marie Skłodowska-Curie program (ref: 101007430) in CICECO-Aveiro Institute of Materials (UIDB/50011/2020; UIDP/50011/2020 and LA/P/0006/2020) financed by national funds through the FCT/MEC (PIDDAC). PhD scholarship of AS is funded by the FCT (2021.07744.BD).

Acknowledgments

We would like to thank Eng. Marta Ferro, senior technician at the Department of Materials and Ceramic Engineering of the University of Aveiro, for her assistance with the STEM analysis and SYNPO (akciová společnost) for providing materials for coatings.

Conflict of interest

The authors declare that the research was conducted in the absence of any commercial or financial relationships that could be construed as a potential conflict of interest.

Publisher's note

All claims expressed in this article are solely those of the authors and do not necessarily represent those of their affiliated organizations, or those of the publisher, the editors and the reviewers. Any product that may be evaluated in this article, or claim that may be made by its manufacturer, is not guaranteed or endorsed by the publisher.

Supplementary material

The Supplementary Material for this article can be found online at: https://www.frontiersin.org/articles/10.3389/fceng.2023.1145049/full#supplementary-material

References

ASTM (2022). *Standard test methods for rating adhesion by tape test, D3359-22*. West Conshohocken, PA: ASTM International.

Augustyniak, A., Tsavalas, J., and Ming, W. (2009). Early detection of steel corrosion via "Turn-On" fluorescence in smart epoxy coatings. *ACS Appl. Mat. Interfaces* 1, 2618–2623. doi:10.1021/am900527s

Bahadur, A., Shoaib, M., Saeed, A., and Iqbal, S. (2016). FT-IR spectroscopic and thermal study of waterborne polyurethane-acrylate leather coatings using tartaric acid as an ionomer. *e-Polymers* 16, 463–474. doi:10.1515/epoly-2016-0154

Bastos, A. C., Karavai, O. V., Zheludkevich, M. L., Yasakau, K. A., and Ferreira, M. G. S. (2010). Localised measurements of pH and dissolved oxygen as complements to SVET in the investigation of corrosion at defects in coated aluminum alloy. *Electroanalysis* 22, 2009–2016. doi:10.1002/elan.201000076

Basu, D., Das, A., Stöckelhuber, K. W., Wagenknecht, U., and Heinrich, G. (2014). Advances in layered double hydroxide (LDH)-based elastomer composites. *Prog. Polym. Sci.* 39, 594–626. doi:10.1016/j.progpolymsci.2013.07.011

Bouali, A. C., Serdechnova, M., Blawert, C., Tedim, J., Ferreira, M. G. S., and Zheludkevich, M. L. (2020). Layered double hydroxides (LDHs) as functional materials for the corrosion protection of aluminum alloys: A review. *Appl. Mat. Today* 21, 100857. doi:10.1016/j.apmt.2020.100857

Braterman, P. S., Tan, C., and Zhao, J. (1994). Orientational effects in the infrared spectrum of the double layer material, magnesium aluminum hydroxide ferrocyanide. *Mat. Res. Bull.* 29, 1217–1221. doi:10.1016/0025-5408(94)90144-9

Cao, L., Wang, Q., Li, Q., and Chen, S. (2022). Synthesis of smart nanofiber coatings with autonomous self-warning and self-healing functions. *ACS Appl. Mat. Interfaces* 14, 27168–27176. doi:10.1021/acsami.2c05048

Cavani, F., Trifirò, F., and Vaccari, A. (1991). Hydrotalcite-type anionic clays: Preparation, properties and applications. *Catal. Today.* 11, 173–301. doi:10.1016/0920-5861(91)80068-K

Chen, Z., Scharnagl, N., Zheludkevich, M. L., Ying, H., and Yang, W. (2023). Micro/nanocontainer-based intelligent coatings: Synthesis, performance and applications – a review. *J. Chem. Eng.* 451, 138582. doi:10.1016/j.cej.2022.138582

Dhole, G. S., Gunasekaran, G., Singh, S. K., and Vinjamur, M. (2015). Smart corrosion sensing phenanthroline modified alkyd coatings. *Prog. Org. Coat.* 89, 8–16. doi:10.1016/j.porgcoat.2015.07.020

Eom, S. H., Kim, S. S., and Lee, J. B. (2020). Assessment of anti-corrosion performances of coating systems for corrosion prevention of offshore wind power steel structures. *Coatings* 10, 970–1014. doi:10.3390/coatings10100970

Exbrayat, L., Salaluk, S., Uebel, M., Jenjon, R., Rameau, B., Koynov, K., et al. (2019). Nanosensors for monitoring early stages of metallic corrosion. *ACS Appl. Nano Mat.* 2, 812–818. doi:10.1021/acsanm.8b02045

Farjana, S. H., Mahmud, M. A. P., and Huda, N. (2021). "Chapter 2 - life cycle assessment in mining industries," in *Life cycle assessment for sustainable mining* (Elsevier), 15–59. doi:10.1016/B978-0-323-85451-1.00002-0

Feldmannová, M., Hilscherová, K., Marsálek, B., and Bláha, L. (2006). Effects of N-heterocyclic polyaromatic hydrocarbons on survival, reproduction, and biochemical parameters in Daphnia magna. *Environ. Toxicol.* 21, 425–431. doi:10.1002/tox.20198

Frankel, G. S., and Zhang, J. (1999). Corrosion-sensing behavior of an acrylic-based coating system. *Corrosion* 55, 957–967. doi:10.5006/1.3283932

Galvão, T. L. P., Sousa, I., Wilhelm, M., Carneiro, J., Opršal, J., Slaná, H., et al. (2018). Improving the functionality and performance of AA2024 corrosion sensing coatings with nanocontainers. *J. Chem. Eng.* 341, 526–538. doi:10.1016/j.cej.2018.02.061

Habib, S., Shakoor, R. A., and Kahraman, R. (2021). A focused review on smart carriers tailored for corrosion protection: Developments, applications, and challenges. *Prog. Org. Coat.* 154, 106218. doi:10.1016/j.porgcoat.2021.106218

Halevy, I., and Bachan, A. (2017). The geologic history of seawater pH. *Science* 355, 1069–1071. doi:10.1126/science.aal4151

Hansen, H. C. B. (1994). Synthesis and properties of hexacyanoferrate interlayered in hydrotalcite. I. Hexacyanoferrate(II). *Clays Clay Min.* 42, 170–179. doi:10.1346/CCMN.1994.0420207

Hogg, S. M., Anderson, B. E., Le Bas, P., and Remillieux, M. C. (2019). Nonlinear resonant ultrasound spectroscopy of stress corrosion cracking in stainless steel rods. *NDT E Int.* 102, 194–198. doi:10.1016/j.ndteint.2018.12.007

Holgado, M. J., Rivers, V., Sanroman, M. S., and Malet, P. (1996). Hexacyanoferrate-interlayered hydrotalcite. *Solid State Ion.* 92, 273–283. doi:10.1016/S0167-2738(96)00478-X

Ikechukwu, E., and Pauline, E. (2015). Environmental impacts of corrosion on the physical properties of copper and aluminium: A case study of the surrounding water bodies in port harcourt. *Open J. Soc. Sci.* 3, 143–150. doi:10.4236/jss.2015.32019

ISO and CEN (2022). *Corrosion tests in artificial atmospheres – salt spray tests ISO 9227: 2022*. Geneva: ISO.

ISO (2020). *Plastics — differential scanning calorimetry (DSC) — Part 2: Determination of glass transition temperature and step height ISO 11357-2: 2020*. Geneva: ISO.

Kirchgeorg, T., Weinberg, I., Hörnig, M., Baier, R., Schmid, M. J., and Brockmeyer, B. (2018). Emissions from corrosion protection systems of offshore wind farms: Evaluation of the potential impact on the marine environment. *Mar. Pollut. Bull.* 136, 257–268. doi:10.1016/j.marpolbul.2018.08.058

Kloprogge, J. T., Wharton, D., Hickey, L., and Frost, R. L. (2002). Infrared and Raman study of interlayer anions CO_3^{2-}, NO_3^-, SO_4^{2-} and ClO_4^- in Mg/Al-hydrotalcite. *Am. Min.* 87, 623–629. doi:10.2138/am-2002-5-604

Koch, G., Varney, J., Thompson, N., Moghissi, O., Gould, M., and Payer, J. (2016). in *International measures of prevention, application, and economics of corrosion technologies (IMPACT) study*. Editor G. Jacobson (Houston: NACE International).

Lewis, R. N., Mc Elhaney, R. N., Pohle, W., and Mantsch, H. H. (1994). Components of the carbonyl stretching band in the infrared spectra of hydrated 1,2-diacylglycerolipid bilayers: A reevaluation. *Biophys. J.* 67, 2367–2375. doi:10.1016/s0006-3495(94)80723-4

Li, W., and Calle, L. M. (2007). "Controlled release microcapsules for smart coatings," in *Nace – int. Corros. Conf. 2007*, 07228.

Liu, C., Jin, Z., Cheng, L., Zhao, H., and Wang, L. (2020). Synthesis of nanosensors for autonomous warning of damage and self-repairing in polymeric coatings. *Nanoscale* 12, 3194–3204. doi:10.1039/C9NR09221H

Low, I. M., and Shi, C. (1998). Vickers indentation responses of epoxy polymers. *J. Mat. Sci. Lett.* 17, 1181–1183. doi:10.1023/A:1006517005082

Lv, J., Yue, Q.-X., Ding, R., Han, Q., Liu, X., Liu, J.-L., et al. (2021a). Construction of zeolite-loaded fluorescent supramolecular on-off probes for corrosion detection based on a cation exchange mechanism. *Nanomaterials* 11, 169. doi:10.3390/nano11010169

Lv, J., Yue, Q.-X., Ding, R., Li, W.-H., Wang, X., Gui, T.-J., et al. (2021b). Intelligent anti-corrosion and corrosion detection coatings based on layered supramolecules intercalated by fluorescent off-on probes. *J. Taiwan Inst. Chem. Eng.* 118, 309–324. doi:10.1016/j.jtice.2020.12.032

Ma, L., Ren, C., Wang, J., Liu, T., Yang, H., Wang, Y., et al. (2021). Self-reporting coatings for autonomous detection of coating damage and metal corrosion: A review. *J. Chem. Eng.* 421, 127854. doi:10.1016/j.cej.2020.127854

Madbouly, S. A., Otaigbe, J. U., Nanda, A. K., and Wicks, D. A. (2005). Rheological behavior of aqueous polyurethane dispersions: Effects of solid content, degree of neutralization, chain extension, and temperature. *Macromolecules* 38, 4014–4023. doi:10.1021/ma050453u

Maia, F., Tedim, J., Lisenkov, A. D., Salak, A. N., Zheludkevich, M. L., and Ferreira, M. G. S. (2012). Silica nanocontainers for active corrosion protection. *Nanoscale* 4, 1287–1298. doi:10.1039/c2nr11536k

Maia, F., Tedim, J., Bastos, A. C., Ferreira, M. G. S., and Zheludkevich, M. L. (2013). Nanocontainer-based corrosion sensing coating. *Nanotechnology* 24, 415502. doi:10.1088/0957-4484/24/41/415502

Martins, R., Figueiredo, J., Sushkova, A., Wilhelm, M., Tedim, J., and Loureiro, S. (2022). Smart" nanosensors for early detection of corrosion: Environmental behavior and effects on marine organisms. *Environ. Pollut.* 302, 118973. doi:10.1016/j.envpol.2022.118973

Melchers, R. E. (2006). Recent progress in the modeling of corrosion of structural steel immersed in seawaters. *J. Infrastruct. Syst.* 12, 154–162. doi:10.1061/(asce)1076-0342(2006)12:3(154)

Montemor, M. F. (2014). Functional and smart coatings for corrosion protection: A review of recent advances. *Surf. Coat. Technol.* 258, 17–37. doi:10.1016/j.surfcoat.2014.06.031

Moshkriz, A., and Darvishi, R. (2022). Preparation and characterization of polyurethane rubber/polypropylene-based thermoplastics vulcanizates nanocomposites with succinic anhydride intercalated layered double hydroxide. *Polym. Polym. Compos.* 30, 096739112210791. doi:10.1177/09673911221079126

Niazi, H., Eadie, R., Chen, W., and Zhang, H. (2021). High pH stress corrosion cracking initiation and crack evolution in buried steel pipelines: A review. *Eng. Fail. Anal.* 120, 105013. doi:10.1016/j.engfailanal.2020.105013

Noël, J.-M., Médard, J., Combellas, C., and Kanoufi, F. (2016). Prussian blue degradation during hydrogen peroxide reduction: A scanning electrochemical microscopy study on the role of the hydroxide ion and hydroxyl radical. *ChemElectroChem* 3, 1178–1184. doi:10.1002/celc.201600196

Olajire, A. A. (2018). Recent advances on organic coating system technologies for corrosion protection of offshore metallic structures. *J. Mol. Liq.* 269, 572–606. doi:10.1016/j.molliq.2018.08.053

Poznyak, S. K., Tedim, J., Rodrigues, L. M., Salak, A. N., Zheludkevich, M. L., Dick, L. F. P., et al. (2009). Novel inorganic host layered double hydroxides intercalated with guest organic inhibitors for anticorrosion applications. *ACS Appl. Mat. Interfaces* 1, 2353–2362. doi:10.1021/am900495r

Priyada, P., Margret, M., Ramar, R., Shivaramu, N. J., Menaka, M., Thilagam, L., et al. (2011). Intercomparison of gamma scattering, gammatography, and radiography techniques for mild steel nonuniform corrosion detection. *Rev. Sci. Instrum.* 82, 035115. doi:10.1063/1.3562893

Raverkar, P., Siddiqui, J. A., Kulkarni, A., and Mulaveesala, R. (2021). "Corrosion detection in mild steel using effective post processing technique for modulated thermal imaging: A numerical study," in Proceeding of the 2021 IEEE International Conference on Technology, Research, and Innovation for Betterment of Society (TRIBES), Raipur, India, December 2021 (IEEE), 1–4. doi:10.1109/TRIBES52498.2021.9751651

Revie, R. W., and Uhlig, H. H. (2008). *Corrosion and corrosion control*. Hoboken, NJ, USA: John Wiley & Sons, Inc. doi:10.1002/9780470277270

Roshan, S., Sarabi Dariani, A. A., and Mokhtari, J. (2018). Monitoring underlying epoxy-coated St-37 corrosion via 8-hydroxyquinoline as a fluorescent indicator. *Appl. Surf. Sci.* 440, 880–888. doi:10.1016/j.apsusc.2018.01.188

Skjolding, L. M., Jørgensen, L. G., Dyhr, K. S., Köppl, C. J., McKnight, U. S., Bauer-Gottwein, P., et al. (2021). Assessing the aquatic toxicity and environmental safety of tracer compounds Rhodamine B and Rhodamine WT. *Water Res.* 197, 117109. doi:10.1016/j.watres.2021.117109

Sousa, I., Quevedo, M. C., Sushkova, A., Ferreira, M. G. S., and Tedim, J. (2020). Chitosan microspheres as carriers for pH-indicating species in corrosion sensing. *Macromol. Mat. Eng.* 305, 1900662. doi:10.1002/mame.201900662

Sui, Y., Liu, X., Bai, S., Li, X., and Sun, Z. (2022). Phosphate loaded layered double hydroxides for active corrosion protection of carbon steel. *Corros. Eng. Sci. Technol.* 57, 7–14. doi:10.1080/1478422X.2021.1976086

Taheri, N., Sarabi, A. A., and Roshan, S. (2022). Investigation of intelligent protection and corrosion detection of epoxy-coated St-12 by redox-responsive microcapsules containing dual-functional 8-hydroxyquinoline. *Prog. Org. Coat.* 172, 107073. doi:10.1016/j.porgcoat.2022.107073

Tan, X., Fan, L., Huang, Y., and Bao, Y. (2021). Detection, visualization, quantification, and warning of pipe corrosion using distributed fiber optic sensors. *Autom. Constr.* 132, 103953. doi:10.1016/j.autcon.2021.103953

Tedim, J., Kuznetsova, A., Salak, A. N., Montemor, F., Snihirova, D., Pilz, M., et al. (2012). Zn–Al layered double hydroxides as chloride nanotraps in active protective coatings. *Corros. Sci.* 55, 1–4. doi:10.1016/j.corsci.2011.10.003

Theerasilp, M., and Crespy, D. (2021). Halochromic polymer nanosensors for simple visual detection of local pH in coatings. *Nano Lett.* 21, 3604–3610. doi:10.1021/acs.nanolett.1c00620

Trovati, G., Sanches, E. A., Neto, S. C., Mascarenhas, Y. P., and Chierice, G. O. (2010). Characterization of polyurethane resins by FTIR, TGA, and XRD. *J. Appl. Polym. Sci.* 115, 263–268. doi:10.1002/app.31096

Tsukada, K., Tomioka, T., Wakabayashi, S., Sakai, K., and Kiwa, T. (2018). Magnetic detection of steel corrosion at a buried position near the ground level using a magnetic resistance sensor. *IEEE Trans. Magn.* 54, 1–4. doi:10.1109/TMAG.2018.2833852

Twite, R. L., and Bierwagen, G. P. (1998). Review of alternatives to chromate for corrosion protection of aluminum aerospace alloys. *Prog. Org. Coat.* 33, 91–100. doi:10.1016/s0300-9440(98)00015-0

Ulaeto, S. B., Rajan, R., Pancrecious, J. K., Rajan, T. P. D., and Pai, B. C. (2017). Developments in smart anticorrosive coatings with multifunctional characteristics. *Prog. Org. Coat.* 111, 294–314. doi:10.1016/j.porgcoat.2017.06.013

Umoren, S. A., and Solomon, M. M. (2019). Protective polymeric films for industrial substrates: A critical review on past and recent applications with conducting polymers and polymer composites/nanocomposites. *Prog. Mat. Sci.* 104, 380–450. doi:10.1016/j.pmatsci.2019.04.002

Wang, J.-P., Wang, J.-K., Zhou, Q., Li, Z., Han, Y., Song, Y., et al. (2018). Adaptive polymeric coatings with self-reporting and self-healing dual functions from porous core–shell nanostructures. *Macromol. Mat. Eng.* 303, 1700616. doi:10.1002/mame.201700616

Weiser, H. B., Milligan, W. O., and Bates, J. B. (1942). X-ray diffraction studies on heavy metal iron-cyanides. *J. Phys. Chem.* 46, 99–111. doi:10.1021/j150415a013

Wilde, R. E., Ghosh, S. N., and Marshall, B. J. (1970). Prussian blues. *Inorg. Chem.* 9, 2512–2516. doi:10.1021/ic50093a027

Wilhelm, M., Quevedo, M. C., Sushkova, A., Galvão, T. L. P., Bastos, A., Ferreira, M., et al. (2020). Hexacyanoferrate-intercalated layered double hydroxides as nanoadditives for the detection of early-stage corrosion of steel: The revival of prussian blue. *Eur. J. Inorg. Chem.* 2020, 2063–2073. doi:10.1002/ejic.202000144

Wu, H., Dave, F., Mokhtari, M., Ali, M. M., Sherlock, R., Mcllhagger, A., et al. (2022). On the application of Vickers micro hardness testing to isotactic polypropylene. *Polymers* 14, 1804. doi:10.3390/polym14091804

Xia, D.-H., Deng, C. -M., Macdonald, D., Jamali, S., Mills, D., Luo, J. -L., et al. (2022). Electrochemical measurements used for assessment of corrosion and protection of metallic materials in the field: A critical review. *J. Mat. Sci. Technol.* 112, 151–183. doi:10.1016/j.jmst.2021.11.004

Yan, S., Chen, L., Dou, X., Qi, M., Du, Q., He, Q., et al. (2015). Toxicity of 8-hydroxyquinoline in cryprinus carpio using the acute toxicity test, hepatase activity analysis and the comet assay. *Bull. Environ. Contam. Toxicol.* 95, 171–176. doi:10.1007/s00128-015-1566-9

Yang, C., Xing, X., Li, Z., and Zhang, S. (2020). A comprehensive review on water diffusion in polymers focusing on the polymer–metal interface combination. *Polymers* 12, 138. doi:10.3390/polym12010138

Yu, W., Du, M., Ye, W., Lv, W., and Zheng, Q. (2014). Relaxation behavior of layered double hydroxides filled dangling chain-based polyurethane/polymethyl methacrylate nanocomposites. *Polymer* 55, 2455–2463. doi:10.1016/j.polymer.2014.03.039

Zhang, Y., Sun, J., Xiao, X., Wang, N., Meng, G., and Gu, L. (2022). Graphene-like two-dimensional nanosheets-based anticorrosive coatings: A review. *J. Mat. Sci. Technol.* 129, 139–162. doi:10.1016/j.jmst.2022.04.032